JOURNAL OF GEOPHYSICAL RESEARCH, VOL. 105, NO. D2, PAGES 2091–2124, JANUARY 27, 2000

# A comparison of single column model simulations of summertime midlatitude continental convection

Steven Ghan,[1] David Randall,[2] Kuan-Man Xu,[2] Richard Cederwall,[3] Douglas Cripe,[2] James Hack,[4] Sam Iacobellis,[5] Stephen Klein,[6] Steven Krueger,[7] Ulrike Lohmann,[8] John Pedretti,[4] Alan Robock,[9] Leon Rotstayn,[10] Richard Somerville,[5] Georgiy Stenchikov,[9] Yogesh Sud,[11] Gregory Walker,[11] Shaocheng Xie,[3] John Yio,[3] and Minghua Zhang[12]

**Abstract.** Eleven different single-column models (SCMs) and one cloud ensemble model (CEM) are driven by boundary conditions observed at the Atmospheric Radiation Measurement (ARM) program southern Great Plains site for a 17 day period during the summer of 1995. Comparison of the model simulations reveals common signatures identifiable as products of errors in the boundary conditions. Intermodel differences in the simulated temperature, humidity, cloud, precipitation, and radiative fluxes reflect differences in model resolution or physical parameterizations, although sensitive dependence on initial conditions can also contribute to intermodel differences. All models perform well at times but poorly at others. Although none of the SCM simulations stands out as superior to the others, the simulation by the CEM is in several respects in better agreement with the observations than the simulations by the SCMs. Nudging of the simulated temperature and humidity toward observations generally improves the simulated cloud and radiation fields as well as the simulated temperature and humidity but degrades the precipitation simulation for models with large temperature and humidity biases without nudging. Although some of the intermodel differences have not been explained, others have been identified as model problems that can be or have been corrected as a result of the comparison.

## 1. Introduction

The parameterization of clouds and cloud processes has long been recognized as a major weakness in climate models. Much effort has therefore been devoted toward the improvement of cloud parameterizations for climate models. The primary testbed of the parameterizations has been the climate models themselves. However, recently the single-column model (SCM) has emerged as an alternate testbed for climate model parameterizations [*Betts and Miller,* 1986; *Iacobellis and Somerville,* 1991; *Randall et al.* 1996].

As the name suggests, an SCM represents a single grid column of a global climate model (GCM), considered in isolation from the rest of the model. Indeed, many SCMs are based upon the same physics code as their parent GCM. The basic idea is to measure the external forcing at work on a column of the atmosphere which corresponds to a single GCM grid column, to use the SCM to compute the cloud formation and radiative transfer processes inside the column, and to evaluate the results produced by the SCM through comparisons with additional observations. The data required to drive SCM simulations include vertical profiles of temperature, water vapor, and condensed water (for initialization), time series of surface temperature, surface pressure, and surface fluxes of sensible and latent heat (for surface boundary conditions), and time series of vertical profiles of the large-scale vertical motion, the large-scale horizontal pressure gradient, and of the tendencies of temperature, water vapor, and con-

[1]Pacific Northwest National Laboratory, Richland, Washington.
[2]Department of Atmospospheric Science, Colorado State University, Fort Collins, Colorado.
[3]Lawrence Livermore National Laboratory, Livermore, California.
[4]National Center for Atmospheric Research, Boulder, Colorado.
[5]Scripps Institution of Oceanography, University of California, La Jolla.
[6]Geophysical Fluid Dynamics Laboratory, Princeton, New Jersey.
[7]Department of Meterology, University of Utah, Salt Lake City, Utah.
[8]Department of Physics and Oceanography, Dalhousie University, Halifax, Nova Scotia.
[9]Rutgers University, New Brunswick, New Jersey.
[10]CSIRO Atmospheric Research, Aspendale, Australia.
[11]Goddard Space Flight Center, Greenbelt, Maryland.
[12]State University of New York, Stony Brook.



Paper number 1999JD900971.
0148-0227/00/1999JD900971$09.00

densed water due to horizontal advection (for lateral boundary conditions).

SCMs can be supplemented with more detailed models, which can be called cloud ensemble models (CEMs) (also known as cloud system models and cloud-resolving models). A CEM explicitly simulates cloud-scale motions, while parameterizing the smaller-scale turbulent motions. CEMs are designed to simulate the cloud-scale processes that must be parameterized in a GCM or SCM. A CEM domain may be considered to represent a GCM grid column, so in a sense, a CEM can be viewed as an "extremely detailed" SCM. For this reason it is useful to evaluate SCM output in part by comparison with CEM output. A CEM typically includes a turbulence parameterization, a bulk ice-phase microphysics parameterization, a cloud microphysics parameterization, and interactive solar and infrared radiation parameterizations. As with an SCM, observed large-scale vertical motion, horizontal advection, and horizontal pressure gradients can be prescribed as forcing functions. The observations of large-scale fields and tendencies required for scientific applications of a CEM are the same as those required by a SCM; with the exception of the advective tendencies of condensed water, these observations can be provided by measurements. CEMs compute some things that are very difficult to observe, such as the vertical distributions of liquid water and ice. This simulated information is no substitute for real observations, because as mentioned above the CEMs do contain parameterizations, notably microphysics, radiation, and turbulence parameterizations, which introduce major uncertainties. Nevertheless, CEM results can be judiciously compared with SCM results in order to diagnose problems with the latter. This strategy for the testing of parameterizations through the use of SCMs and CEMs has been embraced by the GEWEX Cloud System Study [*GCSS Science Team*, 1993; *Moncrieff et al.*, 1997] (GEWEX is the Global Energy and Water Experiment) [see *Browning*, 1993] and also by the Atmospheric Radiation Measurement (ARM) program , which is sponsored by the U.S. Department of Energy.

Providing the necessary SCM and CEM lateral boundary conditions from measurements has proven to be extremely challenging, largely because of sampling and measurement errors in the winds [*Zhang and Lin*, 1997; *Mace and Ackerman*, 1996; *Randall et al.*, 1996]. In addition, for highly advective conditions the lack of cloud measurements along the lateral boundaries can degrade the accuracy of the simulation in the interior of the single column [*Petch and Dudhia*, 1998]; under such conditions the clouds are largely controlled by the lateral boundary conditions, so an SCM is not a suitable testbed for cloud parameterizations.

Yet the SCM is an attractive alternative to the GCM as a parameterization testbed for two reasons. First, the SCM runs much faster than a GCM and hence can be used to quickly test new parameterizations. By judiciously selecting an SCM domain that experiences a wide range of meteorological conditions, a parameterization developer can use an SCM to test a scheme under climatic conditions found in much if not most of the world, without the computational burden of global simulations. Second, SCM simulations can be much shorter than the GCM simulations. By initializing and forcing SCM simulations with observed conditions, a parameterization developer can compare SCM simulations with daily or even hourly observations, providing an almost immediate test of the parameterization for the conditions of interest. SCM simulations are therefore typically days to weeks rather than months to years.

There are however, several issues that must be addressed before SCMs can be used systematically for parameterization evaluation and development. These issues are related to the selection of an optimal methodology for using SCMs as parameterization testbeds. The first purpose of this paper is therefore to evaluate different methodologies for using SCMs as parameterization testbeds. These methodologies involve (1) the analysis procedure used to provide the lateral boundary conditions for the simulations, (2) the treatment of the lower boundary conditions in the simulations, and (3) the treatment of the vertical and horizontal advective tendencies in the simulations, given the lateral boundary conditions.

Although multiple models will be used to explore these issues because the response of one particular model is not necessarily representative of the response of others, the purpose of this paper is not to completely resolve and understand differences between results of different models. Given the many ways in which different models can represent a variety of atmospheric processes, it is likely that a complete reconciliation of simulations by different models will require a systematic substitution of the parameterizations of each process. Such a study is beyond the scope of this paper. However, in some cases it is possible to identify the causes of differences between simulations by models that are similiar in many respects. The identification of the causes of the differences can lead to improvements in particular models. Thus the second purpose of this paper is to understand differences between simulations by different models, to the extent possible without systematically replacing parameterizations of every process.

If the ultimate goal of single-column modeling is the development of parameterizations of atmospheric processes, then comparisons with independent observations are essential. The third purpose of this paper is therefore to use the comparison of simulations with observations to identify model weaknesses and their causes. In some cases this can be rather easily accomplished, but in others it can prove to be quite difficult, particularly given the uncertainty in the forcing used to drive the model simulations. Although some model weaknesses

and their causes have been identified, others will require further experimentation that is beyond the scope of this paper.

In this study we have brought together a collection of 11 SCMs and one CEM and subjected each of them to several alternative analyses of the large-scale forcing observed over the ARM site in the southern Great Plains (SGP) [*Stokes and Schwartz,* 1994] during the intensive observation period (IOP) July 18 to August 3, 1995. It is worth noting that most evaluations of parameterizations using the SCM framework have been performed in tropical latitudes, where horizontal advection plays only a very minor role in driving cloud formation. Although horizontal advection generally plays a weaker role during summertime than wintertime at a midlatitude continental site, it is typically stronger during the summertime at the midlatitude site than at anytime in the tropics. This study should be regarded as a step toward SCM evaluation studies under the highly advective conditions characteristic of wintertime midlatitudes.

Section 2 describes the different analyses and the data used in the analyses and in the model evaluation. Section 3 describes the models. The baseline experiment is analyzed in section 4, which is followed by an evaluation of sensitivity experiments in section 5. Conclusions are summarized in section 6.

## 2. Approach

### 2.1. Experiment Design

As mentioned in the introduction, this study involves the evaluation and comparison of a dozen models at the ARM site in the southern Great Plains during the IOP July 18 to August 3, 1995. For each model the conservation equations in pressure coordinates for the site-wide mean potential temperature, water vapor mixing ratio, and the cloud water and cloud ice mixing ratios have the same form:

$$\frac{\partial \bar{q}}{\partial t} = \left(\frac{\partial \bar{q}}{\partial t}\right)_{\text{L.S}} - \frac{\partial \overline{q'\omega'}}{\partial p} + P_q, \qquad (1)$$

where

$$\left(\frac{\partial \bar{q}}{\partial t}\right)_{\text{L.S.}} \equiv -\left(\bar{\mathbf{v}} \cdot \nabla \bar{q} + \bar{\omega}\frac{\partial \bar{q}}{\partial p}\right) \qquad (2)$$

is the large-scale advective tendency of $\bar{q}$. In these equations, $q$ represents either potential temperature, water vapor mixing ratio, or cloud water or cloud ice mixing ratios; an overbar indicates a site-wide average, $\nabla$ is the horizontal del operator, $\overline{q'\omega'}$ represents the subgrid transport by turbulence and cumulus convection, and $P_q$ represents the condensation, evaporation, and radiative heating that affects $\bar{q}$.

As mentioned in the introduction, there are several issues involved in the methodology for using SCMs as parameterization testbeds. One issue involves the analysis procedure used to provide the lateral boundary conditions for the simulations. Should the forcing fields that drive the SCM simulation be prescribed from objective analyses (which do not employ physical parameterizations but may employ conservation principles) or from operational weather forecast analyses (which uses physical parameterizations as well as conservation principles)? In many regions of the world where data density is low, operational analysis is the only viable option. Even at the ARM southern Great Plains site, where the density of measurements is particularly high, there are questions about the sufficiency of the measurement density for objective analysis [*Mace and Ackerman,* 1996]. For this reason, objective analysis is only used in regions with high data density [*Betts and Miller,* 1986], while operational analysis is used in data-sparse regions [*Iacobellis and Somerville,* 1991; *Randall et al.*, 1996].

Objective analysis will be used in this study because the measurement density at the ARM SGP site is high. To explore the dependence of the simulations on the particular objective analysis method, two different methods will be considered. The baseline method applies conservation of column mass, water vapor, and energy to the analyzed winds, temperature, and humidity, while the second method applies only conservation of column mass. These two objective analysis methods, referred to as SUNY and LLNL, respectively, are described in more detail in section 2.3.

A second methodological issue involves the treatment of the lower boundary condition in the simulations. Most SCMs and CEMs are designed to calculate the turbulent fluxes of sensible and latent heat at the surface. Although allowing the models to calculate the surface fluxes has some advantages (which will be explored in a subsequent study), the fluxes are prescribed in this study because the focus is on the evaluation of cloud and radiation parameterizations. However, as shown by *Doran et al.* [1998], estimate of the spatial mean surface fluxes from direct measurements across even a relatively homogeneous region such as the ARM SGP site requires measurements at representative sites that may not be available. To test the sensitivity of the model simulations to the prescription of the surface fluxes, two different estimates of the site-wide mean surface fluxes are used to drive the model simulations in this study. The baseline estimate uses the SiB2 land-surface model simulations driven by ARM surface and satellite measurements on a 6.25 km grid [*Doran et al.* 1998]. A second estimate is based on measurements at 10 energy balance Bowen ratio (EBBR) stations in the ARM SGP domain (see section 2.2). As noted by *Doran et al.*, the differences between these two estimates of the site-wide mean surface fluxes are quite large.

A third methodological issue involves the treatment of the large-scale vertical and horizontal advective tendencies in the simulations, given the lateral boundary conditions. Since the objective analyses provide es-

timates of both the site-wide mean winds (horizontal $\bar{\mathbf{v}}_{\mathrm{obs}}$ and vertical $\bar{\omega}_{\mathrm{obs}}$) and the site-wide mean advective tendencies (horizontal $-(\bar{\mathbf{v}}\cdot\nabla\bar{q})_{\mathrm{obs}}$ and vertical $-\left(\bar{\omega}\frac{\partial\bar{q}}{\partial p}\right)_{\mathrm{obs}}$), the models can be driven either by the analyzed winds or by the analyzed advective tendencies. (The models are not strictly driven by the lateral boundary conditions but rather by the large-scale advective tendencies, which are assumed to be uniform throughout each model layer and are derived from the objective analyses). In the former case the model is allowed to estimate the advective tendency from the analyzed wind and the simulated gradient of the advected field (temperature or humidity). For vertical advection the model would use the simulated vertical profile of the advected field. For horizontal advection, *Randall and Cripe* [1999] showed that for an upstream advection scheme, horizontal advection acts like a relaxation of the simulated site-wide mean field $\bar{q}$ toward the analyzed inflow value $\bar{q}_{\mathrm{in}}$ (i.e., the value of the upwind grid cell) with a relaxation time-scale $\tau_{\mathrm{adv}}$, so the large-scale advective tendency of $\bar{q}$ can be written (in pressure coordinates) as

$$\left(\frac{\partial\bar{q}}{\partial t}\right)_{\mathrm{L.S.}} = -\frac{\bar{q}-\bar{q}_{\mathrm{in}}}{\tau_{\mathrm{adv}}} - \left(\bar{\omega}\frac{\partial\bar{q}}{\partial p}\right)_{\mathrm{obs}} \tag{3}$$

where

$$\tau_{\mathrm{adv}} \approx \frac{d}{2V}, \tag{4}$$

with $V$ the average wind speed in the region (in this case, in the ARM SGP domain) and $d$ a length scale (specified here as 300 km) which is closely related to the distance across the region. *Randall and Cripe* [1999] showed that the total advective tendency can also be written as

$$\left(\frac{\partial\bar{q}}{\partial t}\right)_{\mathrm{L.S.}} = -(\bar{\mathbf{v}}\cdot\nabla\bar{q})_{\mathrm{obs}} - \frac{\bar{q}-\bar{q}_{obs}}{\tau_{\mathrm{adv}}} - \left(\bar{\omega}\frac{\partial\bar{q}}{\partial p}\right)_{\mathrm{obs}}, \tag{5}$$

where $\bar{q}_{obs}$ is the analyzed field averaged across the site. Thus the model can treat the dependence of the horizontal advective tendency on the simulated field by simply adding a nudging term, with the nudging time-scale given by the time-scale for horizontal advection across the domain.

In this study, three different treatments of advection are used. In the baseline experiment both the horizontal and the vertical advective tendencies of temperature and humidity are prescribed from the analysis,

$$\left(\frac{\partial\bar{q}}{\partial t}\right)_{\mathrm{L.S}} = -\left(\bar{\mathbf{v}}\cdot\nabla\bar{q} + \bar{\omega}\frac{\partial\bar{q}}{\partial p}\right)_{\mathrm{obs}}. \tag{6}$$

This ensures that all models are driven by the same advective tendencies for temperature and water vapor; for cloud water and cloud ice the horizontal advection is neglected for lack of observations, and the vertical advection is either neglected (in some models) or calculated from the analyzed vertical velocity and the simulated vertical profile of cloud water and cloud ice mixing ratio.

In a second treatment, nudging is applied to the horizontal advective tendency as described above, with the vertical advective tendency prescribed from the analysis. Although nudging can hide errors in the parameterization to be evaluated [*Ghan et al.*, 1999; *Randall and Cripe*, 1999], it can also suppress sensitive dependence on initial conditions [*Hack and Pedretti,* 1999] and correct for errors in the analyzed advective tendencies.

In the third treatment the horizontal advective tendency is prescribed, but the vertical advective tendency is calculated from the simulated profile of the advected field,

$$\left(\frac{\partial\bar{q}}{\partial t}\right)_{\mathrm{L.S.}} = -(\bar{\mathbf{v}}\cdot\nabla\bar{q})_{\mathrm{obs}} - \bar{\omega}_{\mathrm{obs}}\frac{\partial\bar{q}}{\partial p}. \tag{7}$$

This treatment can potentially suppress the production of negative water vapor concentrations by allowing the vertical transport to depend on the simulated water vapor profile.

Altogether a total of five experiments is presented in this paper: the baseline experiment (denoted baseline), an experiment (denoted LLNL) in which the models are driven by the LLNL objective analysis rather than by the SUNY objective analysis, an experiment (denoted EBBR) in which the EBBR surface fluxes rather than the SiB2 surface fluxes are used to drive the simulations, an experiment (denoted nudging) in which nudging of temperature and humidity is applied, and an experiment (denoted VADV) in which the vertical advective tendency is calculated from the analyzed vertical velocity and the simulated vertical profiles of the advected fields. The characteristics of these experiments are summarized in Table 1.

In each experiment all models are initialized with the same analyzed vertical profiles of site-wide mean temperature, water vapor mixing ratio, and horizontal wind velocity. Measurements of vertical profiles of cloud liquid water and cloud ice are not available for the time period of the simulations, so the models were initialized with no clouds. For radiative transfer calculations, the surface temperature was specified on the basis of the same observations for all models, but the albedo and emissivity were taken from the particular representation of the surface by each model. Radiative transfer calculations that required temperature, water vapor mixing ratio, and ozone mixing ratio profiles above 20 km used the "standard midlatitude summer atmosphere" profiles. Radiative transfer calculations used a time-varying top-of-atmosphere downwelling solar flux calculated for the central facility of the ARM SGP, which is located at latitude 36° 36′ N, longitude 97° 29′ W. Profiles of the large-scale forcing terms were given at 10 mbar intervals for the LLBL objective analyses and at 50 mbar intervals for the SUNY objective analyses. Both were supplied at 3 hour time intervals.

**Table 1.** Characteristics of Experiments Considered in This Study.

| | Baseline | LLNL | EBBR | Nudging | VADV |
|---|---|---|---|---|---|
| Objective analysis | SUNY | LLNL | SUNY | SUNY | SUNY |
| Surface fluxes | SiB2 | SiB2 | EBBR | SiB2 | SiB2 |
| Vertical advection | $-\left(\bar{\omega}\frac{\partial \bar{q}}{\partial p}\right)_{\rm obs}$ | $-\left(\bar{\omega}\frac{\partial \bar{q}}{\partial p}\right)_{\rm obs}$ | $-\left(\bar{\omega}\frac{\partial \bar{q}}{\partial p}\right)_{\rm obs}$ | $-\left(\bar{\omega}\frac{\partial \bar{q}}{\partial p}\right)_{\rm obs}$ | $-\left(\bar{\omega}_{\rm obs}\frac{\partial \bar{q}}{\partial p}\right)$ |
| Horizontal advection | $-(\bar{\mathbf{v}}\cdot\nabla\bar{q})_{\rm obs}$ | $-(\bar{\mathbf{v}}\cdot\nabla\bar{q})_{\rm obs}$ | $-(\bar{\mathbf{v}}\cdot\nabla\bar{q})_{\rm obs}$ | $-(\bar{\mathbf{v}}\cdot\nabla\bar{q})_{\rm obs}-\frac{\bar{q}-\bar{q}_{obs}}{\tau_{\rm adv}}$ | $-(\bar{\mathbf{v}}\cdot\nabla\bar{q})_{\rm obs}$ |

For the simulations reported in this paper each model was run with its own vertical resolution and time step (see section 3). Simulations with the CEM used a domain size of 512 km and a horizontal grid size of 2 km. The vertical coordinate was stretched to give finer resolution near the surface, with 33 layers. The two-dimensional CEM domain was oriented along an east-west plane. The lateral boundary condition is cyclic, which is consistent with imposing a horizontally uniform large-scale advective tendency. The large-scale advective tendency of horizontal momentum and the large-scale horizontal pressure gradient force are prescribed from the objective analyses. The initial conditions were horizontally uniform. Cloud-scale circulations were initiated by introducing small random perturbations in the temperature field in the boundary layer for the first hour or so. *Xu and Randall* [1998] describe the CEM setup and results in more detail than is possible here.

### 2.2. Data

Data are required for driving the model simulations and for evaluating the simulations. In principle, the data used to evaluate the simulations should be independent of the data used to drive the simulation. In practice, this is not strictly true for the SUNY objective analysis (described in section 2.3), which requires measurements of column mean temperature, the column water vapor, the column liquid water, and the radiative fluxes at the surface and top of the atmosphere. These measurements are required to enforce the constraints of conservation of column heat and moisture. Although this might appear to compromise the independent evaluation of the simulations, the measurements of each of the above fields does not constrain the models to simulate similar values because the measurements are combined into only two constraints (conservation of column heat and moisture). The models are therefore free to simulate values of column mean temperature, the column water vapor, the column liquid water, and the radiative fluxes at the surface and top of the atmosphere which are, as will be shown in this paper, quite different from the measured values.

The ARM SGP clouds and radiation testbed (CART) provides an unusually dense network of meteorological measurements. The 365 km × 300 km site (Figure 1) includes a central facility, four boundary facilities, and 23 extended facilities. The central facility, which is where most of the instrumentation is deployed, is located near Lamont in north central Oklahoma (36°36'N, 97°29'W, 320 m above sea level), 50 km south of the Kansas border. The central facility instrumentation includes a wide array of conventional and state-of-the-science observing systems that perform the following functions: make radiometric measurements; furnish vertical profiles of wind, temperature, and water vapor (also vertical integrals); quantify the cloud cover, cloud liquid water and ice mixing ratios, and atmospheric aerosols; and permit the calculation of the surface fluxes of heat, moisture, and momentum. Each of the four boundary facilities is located near the midpoint of one side of the CART rectangle (North: Hillsboro, Kansas; West: Vici, Oklahoma; South: Purcell, Oklahoma; East: Morris, Oklahoma). Their instrumentation suites are limited to a sonde system and microwave radiometer, with the resulting wind, temperature, and water vapor profiles providing the basis for the estimation of the lateral fluxes of moisture and energy into and out of the atmospheric volume above the CART rectangle, along with the divergence and tendencies of atmospheric properties for that volume. The 23 extended facilities are distributed reasonably evenly across the CART rectangle. Their instrumentation systems furnish data streams that facilitate the spatial integration of the surface heat, moisture, and momentum fluxes across the CART site.

As discussed in section 2.1, the surface sensible and latent heat fluxes are prescribed in the simulations from two different estimates. One estimate is based on measurements from a network of 10 EBBR stations at the ARM SGP site. The second estimate is based upon 6.25 km resolution simulations by the SiB2 land surface model [*Sellers et al.*, 1986, 1996]. The SiB2 simulations were driven by relatively dense (as fine as 1 km for some input variables) measurements of soil type, vegetation type, leaf area, surface air temperature and humidity, wind speed, insolation, and precipitation, all interpolated to a 6.25 km grid covering the SGP site [*Doran et al.*[1998]. The fluxes simulated by SiB2 were then averaged over the SGP domain.

The lateral boundary conditions required to drive the SCM simulations are derived from analyses of profiles of temperature, humidity, and horizontal velocity mea-

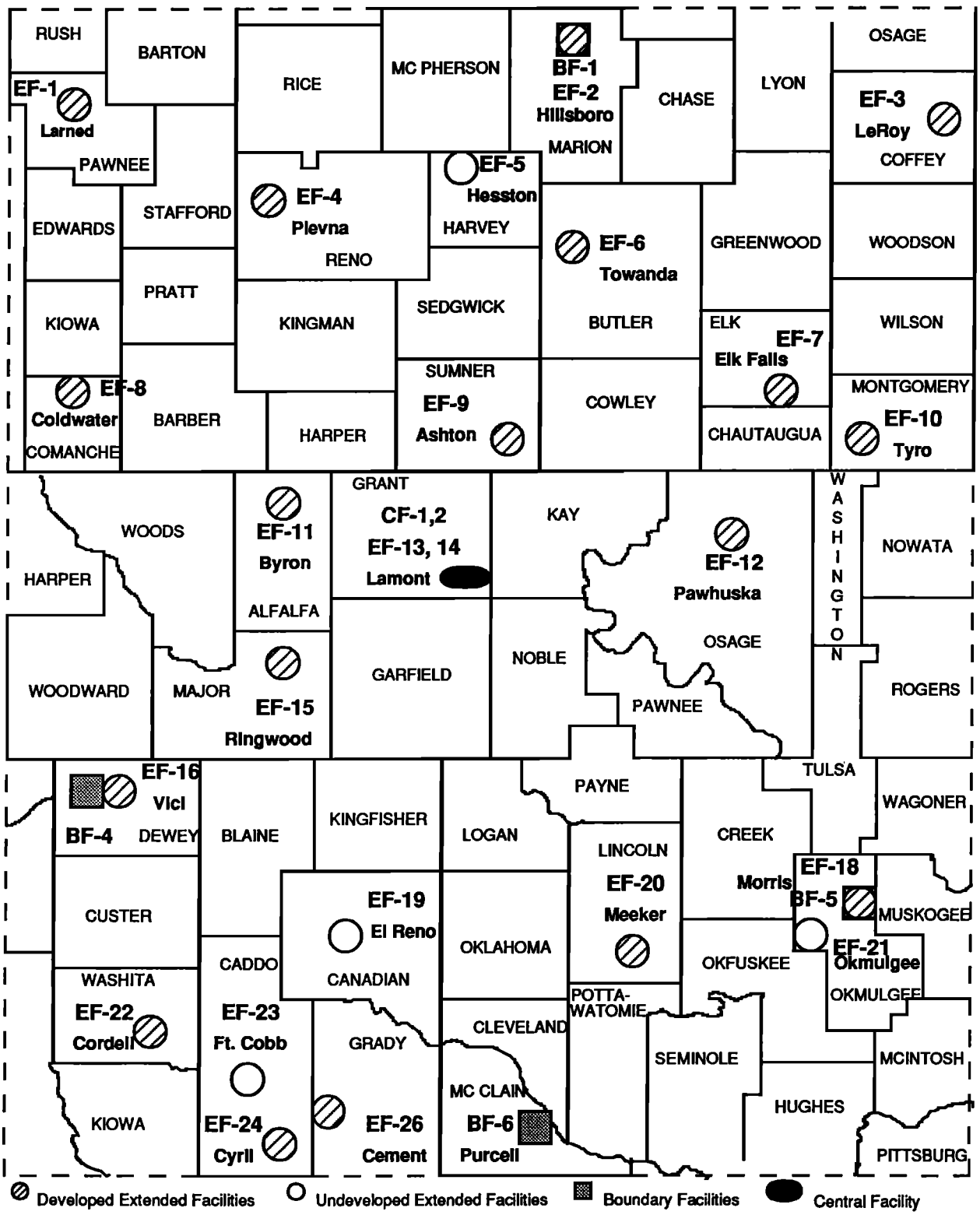


**Figure 1.** ARM southern Great Plains (SGF) site as of August 1995 (courtesy of Argonne National Laboratory).

sured by radiosondes released from the central facility and four boundary facilities every 3 hours of the IOP. The analyses are described in section 2.3.

The observations used to evaluate the model simulations (and to constrain the SUNY analysis of the lateral boundary conditions) consist of Earth radiation budget estimates from National Oceanic and Atmospheric Administration (NOAA) Geostationary Operational Environmental Satellite (GOES 7) measurements, surface radiation budget measurements by ARM Solar and In-

**Table 2.** Model Investigators and References

| Model | Investigator | Reference |
|---|---|---|
| CCCma SCM | Lohmann | *Lohmann et al.*, [1999] |
| CSIRO SCM | Rotstayn | *Rotstayn* [1997], *Rotstayn et al.* [1999] |
| CSU SCM | Randall/Cripe | http://kiwi.atmos.colostate.edu/BUGS.html, *Randall and Cripe* [1999] |
| ECHAM SCM | Lohmann | *Roeckner et al.* [1996], *Lohmann and Roeckner* [1996] |
| GFDL SCM | Klein | see Tables 5–9 |
| McRAS SCM | Sud/Walker | *Takacs et al.* [1994], *Sud and Walker* [1999a,b] |
| NCAR CCM3 SCM | Hack/Pedretti | http://www.cgd..ucar.edu/cms/sccm/scm.html, *Hack et al.* [1998]; *Kiehl et al.* [1998] |
| PNNL/CCM2 SCM | Ghan | *Hack et al.* [1993], *Ghan et al.* [1997] |
| Rutgers SCM | Stenchikov/Robock | *Stenchikov and Robock* [1995] |
| Scripps SCM | Iacobellis/Somerville | see Tables 5–9 |
| SUNY/CCM3 SCM | Xie/Zhang | *Hack et al.* [1998], *Kiehl et al.* [1996], *Xie* [1998] |
| UCLA/CSU CEM | Xu | *Krueger* [1988], *Xu and Krueger*, [1991], *Xu and Randall* [1995] |

frared Radiation Observation Stations (SIROS), estimates of column water vapor and column cloud liquid water from microwave radiometer (MWR) measurements, and precipitation measurements at 47 Oklahoma Mesonet and 5 Surface Meteorological Observing System (SMOS) stations.

The GOES-7 visible and infrared radiance measurements have been converted to hourly 0.5° latitude-longitude gridded broadband fluxes by *Minnis et al.* [1995, 1998]. The flux estimates were then averaged over the CART domain.

The SIROS instruments consist of pyranometers to measure the downwelling and upwelling hemispheric solar flux and of pyrgeometers to measure the downwelling and upwelling hemispheric broadband infrared flux. SIROS instrumentation is deployed at four extended facilities within the CART domain. Area and hourly means of the 15 s measurements are formed from simple arithmetic means of the available observations, filtering out values outside the geophysically realistic bounds of 10-600 W $m^{-2}$ for downwelling and upwelling infrared flux, -10–1600 W $m^{-2}$ for downwelling solar flux, and -10–100 W $m^{-2}$ for upwelling solar flux.

Hourly CART-area mean precipitation rates were formed from the 5 min Oklahoma Mesonet and 30 minute SMOS measurements.

Surface fluxes of sensible and latent heat were measured every 30 minutes by a suite of 10 EBBR stations located at the central and extended CART facilities. CART domain means were formed after outlier values were discarded from the individual station data.

Hourly means of column water vapor and column cloud liquid water were formed from 5 min averages of estimates from microwave radiometer measurements at the central and two boundary CART facilities. Uncertainty in the column water vapor and cloud liquid water is estimated to be 0.5 kg $m^{-2}$ and 0.03 kg $m^{-2}$, respectively [*Lesht and Liljegren,* 1997]. Data are treated as missing when rain is standing on the instrument.

### 2.3. Analysis

Observations cannot be used directly to drive single-column models. Sampling errors and measurement errors are both large enough to dominate the signal in the vertical velocity averaged over a domain the size of a GCM grid cell. Some form of objective analysis

**Table 3.** Model Notation

| Model | Full Name |
|---|---|
| CCCma SCM | Canadian Centre for Climate Modelling and Analysis |
| CSIRO SCM | Commonwealth Scientific and Industrial Research Organization Mark 3 (developmental) |
| CSU SCM | Colorado State University |
| ECHAM SCM | Hamburg version of European Center for Medium-Range Weather Forecasts |
| GFDL SCM | Geophysical Fluid Dynamics Laboratory |
| McRAS SCM | Microphysics of clouds / relaxed Arakawa-Schubert scheme |
| NCAR CCM3 SCM | National Center for Atmospheric Research single-column version of the Community Climate Model Version 3 |
| PNNL/CCM2 SCM | Pacific Northwest National Laboratory version of NCAR CCM2 |
| Rutgers SCM | Rutgers University |
| Scripps SCM | Scripps Institution of Oceanography |
| SUNY/CCM3 SCM | State University of New York at Stony Brook version of NCAR CCM3 |
| UCLA/CSU CEM | University of California at Los Angeles/Colorado State University |

**Table 4.** Model Numerics

| Model | Numerical Domain | Time Step |
|---|---|---|
| CCCma SCM | 19 levels | 1200 s |
| CSIRO SCM | 18 levels | 1800 s |
| CSU SCM | 17 levels | 900 s |
| ECHAM SCM | 19 levels | 1200 s |
| GFDL SCM | 18 levels | 1800 s |
| McRAS SCM | 20 levels | 600 s |
| NCAR CCM3 | 18 levels | 1200 s |
| PNNL/CCM2 SCM | 24 levels | 1200 s |
| Rutgers SCM | 12 levels | 3600 s |
| Scripps SCM | 20 levels | 450 s |
| SUNY/CCM3 SCM | 18 levels | 1200 s |
| UCLA/CSU CEM | 256 x 34 grid points 512 x 20 km domain | 10 s |

is therefore required to ensure that basic conservation properties are not violated in the forcing data. In this paper we consider two different objective analysis techniques.

The Lawrence Livermore National Laboratory (LLNL) objective analysis scheme is based on the method originally proposed by *Barnes* [1964] and subsequently used and documented by many others [*Leach et al.*, 1997]. *Caracena*'s [1987] formulation is used to obtain the spatial derivatives. For application at the SGP site, the temperature and moisture observations from radiosondes at approximately 10 m vertical resolution are processed into 10 hPa layers from 960 hPa to 100 hPa for each of the five simultaneous soundings. Wind observations from the soundings are merged with those from neighboring National Weather Service wind profilers to provide wind fields for the 10 hPa layers. Objective analyses are then performed on these layer-averaged data to provide values of site-wide means and spatial derivatives at 3 hour intervals. Values of winds and spatial derivatives are used to estimate advective tendencies of temperature and moisture. Divergence of the horizontal wind for each layer is integrated, applying *O'Brien*'s [1970] correction, to obtain estimates of large-scale vertical motion.

The State University of New York, Stony Brook (SUNY) objective scheme is based on the variational analysis of *Zhang and Lin* [1997]. It begins with an objective scheme that is similar to the LLNL scheme for smoothing and filling raw input data. It then uses a variational method to adjust the atmospheric state variables (winds, temperature, and humidity) by the minimum possible amount to conserve column-integrated mass, water vapor, and energy. To satisfy the column-integrated mass, water vapor and energy budgets, measurements of the column storage and of the surface and top-of-the-atmosphere fluxes are required. These measurements are described in section 2.2. For the two different estimates of the surface sensible and latent heat fluxes, two different SUNY objective analyses were performed, yielding an analysis at 50hPa pressure intervals every 3 hours. The technical details of the variational procedure and discussion of the required adjustments can be found in the work of *Zhang and Lin* [1997].

For the analysis of the July 1995 ARM IOP data, several augmentations are made to the method described by *Zhang and Lin* [1997]. The first is the introduction of some auxiliary boundary grids to better define the SCM domain at the SGP site. In addition to the four sounding boundary facilities, six NOAA wind profilers are used in defining the SCM domain. The second improvement is the use of background fields from the operational mesoscale analysis of the National Center for Environmental Prediction rapid update cycle model

**Table 5.** Stratiform Cloud Schemes

| Model | Stratiform Cloud Scheme |
|---|---|
| CCCma SCM | prognostic cloud liquid water, cloud ice and cloud droplet number diagnostic cloud fraction |
| CSIRO SCM | prognostic cloud liquid water and cloud ice; statistical cloud fraction |
| CSU SCM | bulk cloud microphysics [*Fowler et al.*, 1996]; cloud fraction is zero or 1 detrainment of condensed water |
| ECHAM SCM | prognostic cloud liquid water and cloud ice; diagnostic cloud fraction detrainment of condensed water |
| GFDL SCM | prognostic liquid and ice [*Rotstayn*, 1997]; prognostic cloud fraction [*Tiedtke*, 1993] detrainment of condensed water |
| McRAS SCM | prognostic cloud scheme [*Sud and Walker*, 1999a,b] prognostic cloud fraction; detrainment of condensed water |
| NCAR CCM3 SCM | diagnostic cloud fraction [*Slingo*, 1987] and condensed water content [*Hack*, 1998] |
| PNNL/CCM2 SCM | prognostic water vapor plus cloud water, cloud ice, ice number [*Ghan et al.*, 1997] no subgrid cloud; detrainment of water vapor plus cloud water |
| Rutgers SCM | cloud water proportional to vapor during condensation *Stenchikov and Robock* [1995] |
| Scripps SCM | prognostic cloud [*Tiedtke*, 1993]; detrainment of condensed water |
| SUNY/CCM3 SCM | diagnostic cloud [*Slingo*, 1987], same as CCM3 |
| UCLA/CSU CEM | three-phase ice microphysics [*Lin et al.*, 1983; *Lord et al.*, 1984; *Krueger et al.*, 1995] |

**Table 6.** Cumulus Convection Schemes

| Model | Cumulus Convection Scheme |
|---|---|
| CCCma SCM | simplified A-S scheme [*Zhang and McFarlane*, 1995] |
| CSIRO SCM | mass flux scheme [*Gregory and Rowntree*, 1990]; convective cloud water |
| CSU SCM | modified A-S scheme [*Pan and Randall*, 1998; *Ding and Randall*, 1998] |
| ECHAM SCM | mass flux scheme [*Tiedtke*, 1989] with an adjustment closure based on CAPE [*Nordeng*, 1994] |
| GFDL SCM | relaxed A-S scheme *Moorthi and Suarez*, 1992] |
| McRAS SCM | relaxed A-S scheme; convective cloud water |
| NCAR CCM3 SCM | *Zhang and McFarlane* [1995], *Hack* [1994] |
| PNNL/CCM2 SCM | CCM2 Mass Flux [*Hack*, 1994] |
| Rutgers SCM | variational convective adjustment [*Stenchikov and Robock*, 1995] |
| Scripps SCM | *Zhang and McFarlane* [1995]; convective cloud water |
| SUNY/CCM3 SCM | modified *Zhang and McFarlane* [1995], *Xie* [1998] |
| UCLA/CSU CEM | none |

in filling missing data. The third is the use of hourly winds at 17 NOAA profilers surrounding the SCM domain. The analysis is also augmented with better estimation of area-mean surface fluxes and precipitation. Description of the impact of these augmentations and the sensitivity of the data products are described in a separate paper [*Zhang et al.*, 1999].

## 3. Summary of models

The 1 single-column models and one two-dimensional cloud ensemble model participating in this comparison are documented in Tables 2–9. The CEM is participating in the study to serve as a reference simulation for those fields that cannot be or have not been observed for the study period; it must be recognized that although the CEM explicitly resolves most convective clouds and hence should provide a superior estimate of cumulus convection, it uses a cloud microphysics parameterization similar to those in SCMs and hence is by no means a perfect reference. The models span a range of spatial resolutions and treatments of physical processes. The number of levels used to represent the atmosphere ranges from 12 to 34. Most models predict cloud condensate, but some (NCAR, SUNY, Rutgers) diagnose the condensate using a prescribed profile under conditions of saturation. Most models treat subgrid cloudiness for stratiform clouds, but the CSU and PNNL models do not. Only the CEM predicts convective cloud condensate, but the CSIRO, McRAS, NCAR, Rutgers, Scripps, and SUNY SCMs diagnose the convective cloud water and relate it to the convective cloud radiative properties; the other SCMs neglect the radiative impact of convective clouds altogether. A variety of deep convection parameterizations are employed in the SCMs, with most using some variant of the Arakawa-Schubert parameterization; the NCAR, Scripps and SUNY SCMs use versions of the *Zhang and McFarlane*, [1995] simplified Arakawa-Schubert parameterization. The Rutgers SCM uses a variational moist convective adjustment scheme. The CSU, ECHAM, McRAS, GFDL, PNNL, and Scripps SCMs treat detrainment of condensed water from cumulus clouds. Most models differ in many respects, making the identification of the causes of intermodel differences in simulations difficult. However, the NCAR and SUNY models differ only in the trigger for cumulus convection [*Xie*, 1998].

**Table 7.** Radiation Schemes

| Model | Radiation Scheme |
|---|---|
| CCCma SCM | LW, *Morcrette* [1989]; SW, *Fouquart and Bonnel* [1980] |
| CSIRO SCM | LW, *Schwarzkopf and Fels* [1991]; SW, *Lacis and Hansen* [1974] |
| CSU SCM | *Harshvardhan et al.* [1987] |
| ECHAM SCM | LW, *Morcrette* [1989]; SW, *Fouquart and Bonnel* [1980] |
| GFDL SCM | LW, *Schwarzkopf and Fels* [1991];SW, *Lacis and Hansen* [1974] |
| McRAS SCM | *Chou et al.*, [1994, 1998, 1999] |
| NCAR CCM3 SCM | *Kiehl et al.*, [1996, 1998] |
| PNNL/CCM2 SCM | LW same as CCM2 [*Hack et al.*, 1993]; SW, same as CCM2 but stratiform cloud properties are parameterized |
| Rutgers SCM | *Stenchikov and Robock* [1995] |
| Scripps SCM | same as ECHAM |
| SUNY/CCM3 SCM | same as CCM3 [*Kiehl et al.*, 1996, 1998] |
| UCLA/CSU CEM | same as CSU SCM |

**Table 8.** Cloud Radiative Properties

| Model | Stratiform Clouds | Convective Clouds |
|---|---|---|
| CCCma SCM | f(LWC,$N_c$,IWC,$N_i$,$\Delta z$) | neglected |
| CSIRO SCM | f(LWC,$N_c$,IWC,$\Delta z$) *Rotstayn* [1997] | f(LWC,$N_c$,IWC,$\Delta z$) |
| CSU SCM | f(LWP,$r_c$,IWP,$r_i$) *Fowler and Randall* [1996] | neglected |
| ECHAM SCM | f(LWC,$N_c$,IWC,$\Delta z$) *Lohmann and Roeckner* [1996] | neglected |
| GFDL SCM | f(LWP,$r_c$,IWP,$r_i$) *Slingo* [1989], *Ebert and Curry* [1992] | neglected |
| McRAS SCM | f(LWC,$N_c$,IWC,$N_i$,$\Delta z$) | f(LWC,$N_c$,IWC,$N_i$,$\Delta z$) |
| NCAR CCM3 SCM | f(LWP,$r_c$,IWP,$r_i$) *Hack* [1998] | f(LWP,$r_c$,IWP,$r_i$) |
| PNNL/CCM2 SCM | f(LWC,$N_c$,IWC,$N_i$,$\Delta z$) *Ghan et al.* [1997] | neglected |
| Rutgers SCM | *Stephens* [1978] | *Stephens* [1978] |
| Scripps SCM | f(LWP,$r_c$,IWP,$r_i$) *Slingo* [1989], *Ebert and Curry* [1992] | f(LWP,$r_c$,IWP,$r_i$) |
| SUNY/CCM3 SCM | same as CCM3 | same as CCM3 |
| UCLA/CSU CEM | f(LWC,$N_c$,IWC,$N_i$) *Xu and Randall* [1995] | f(LWC,$N_c$,IWC,$N_i$) |

## 4. Baseline Experiment

This investigation focuses on the period July 18 to August 3, 1995. Meteorological conditions during the summer 1995 SCM IOP were typical of the continental summertime regime. The first half of the period was characterized by variable cloudiness and precipitation every other day associated with a stationary, large-scale upper level trough over North America. In the second half of the period, upper level ridging led to clear days and hot, dry conditions. An upper level trough replaced the ridge, with increasing cloudiness, thunderstorms, and occasional intense precipitation toward the end of the study period. Hence a wide range of summertime weather conditions occurred for testing SCMs, including hot, clear days, variable cloudiness and local convection, and synoptic forcing with increased cloudiness, precipitation, and occasional severe weather. Inspection of an animation of the satellite images for the IOP reveals the importance of cloud advection through the study area; cloud processes were not governed simply by local convection.

The baseline experiment consists of SCM and CEM simulations driven by the total advective forcing calculated by the SUNY objective analysis, with surface fluxes estimated by the SiB2 model using the [*Doran et al.* [1998] surface analysis.

Plates 1 and 2 show the temperature and specific humidity forcing tendencies as functions of pressure and time. The temperature forcing is marked by periods of 15–30°/d cooling at pressures between 300 and 600 hPa on July 20, 22, 24, 26 and August 1–3, with forcing weaker than 5°/d most other times and pressure levels. The humidity forcing reflects some of the same features as the temperature forcing, with moistening at the same times and pressure levels as the strong cooling, but also exhibits strong drying in the lower troposphere at times, particularly on July 23, 27, and 28.

How do the temperature and humidity fields respond to the forcing? Plate 3 compares the simulated and observed column mean (between pressure levels 100-900 hPa) temperature during the 17 day IOP. Several points are worth noting. First, simulated temperatures drift by up to 15°during the 17 day period. Because the drift is different for each model, it probably reflects model deficiencies rather than limitations in the large-scale forcing used to drive the models, although sensitive dependence on initial conditions [*Hack and Pedretti,* 1999] could also drive some of the differences. Second, all of the simulations exhibit more temporal variability than

**Table 9.** Turbulence Schemes

| Model | Turbulence Scheme |
|---|---|
| CCCma SCM | *Abdella and McFarlane* [1997] |
| CSIRO SCM | *Smith* [1990] modification of *Louis* [1979] K theory |
| CSU SCM | *Suarez et al.* [1983] |
| ECHAM SCM | *Brinkop and Roeckner* [1995] |
| GFDL SCM | 2.5 order, Mellor-Yamada [*Helfand and Lebraga,* 1988] |
| McRAS SCM | same as GFDL SCM |
| NCAR CCM3 SCM | nonlocal bulk [*Holtslag and Boville,* 1993; *Kiehl et al.*, 1998] |
| PNNL/CCM2 SCM | *Smith* [1990] modification of CCM2 [*Hack et al.*, 1993] |
| Rutgers SCM | *Stenchikov and Robock* [1995] |
| Scripps SCM | same as CCM3 |
| SUNY/CCM3 SCM | same as CCM3 |
| UCLA/CSU CEM | 3-order closure [*Krueger,* 1988] |

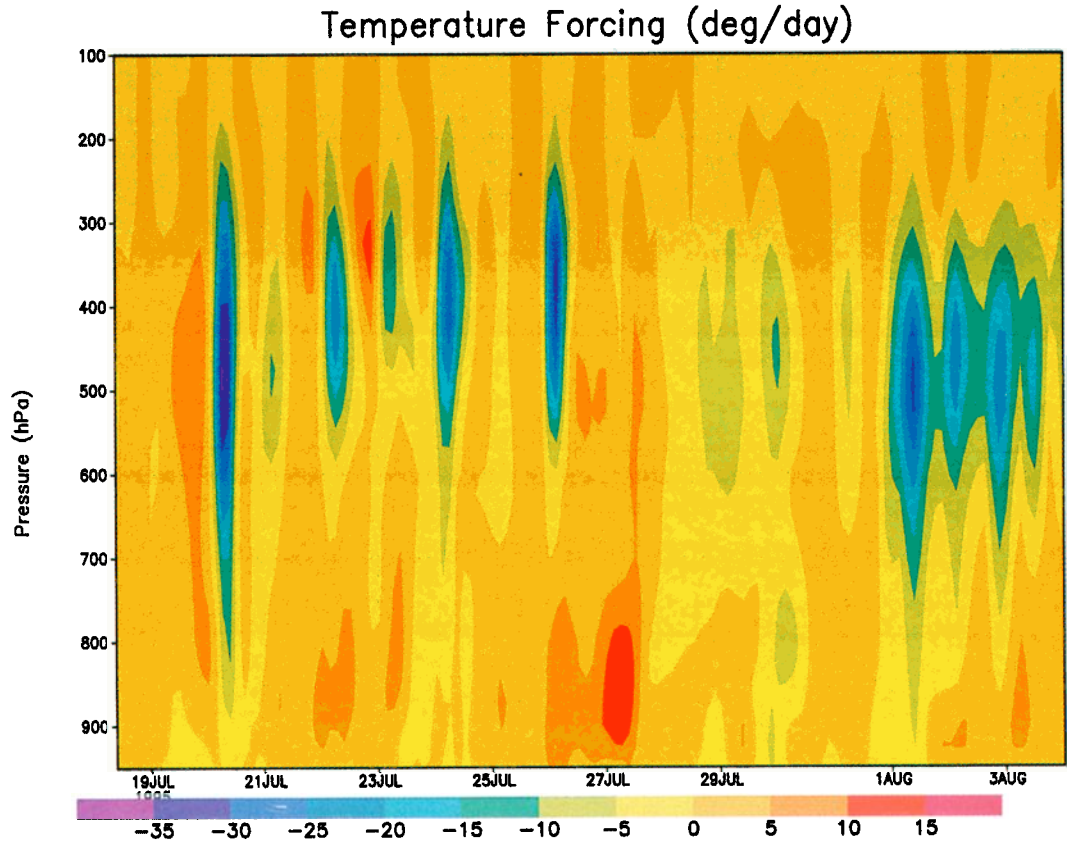


**Plate 1.** Vertical profile of the temperature forcing (°/d) due to horizontal advection, vertical advection, and adiabatic expansion, derived from the SUNY variational analysis (using SiB2 surface fluxes) for the SGP site during the period July 18 to August 3 1995.

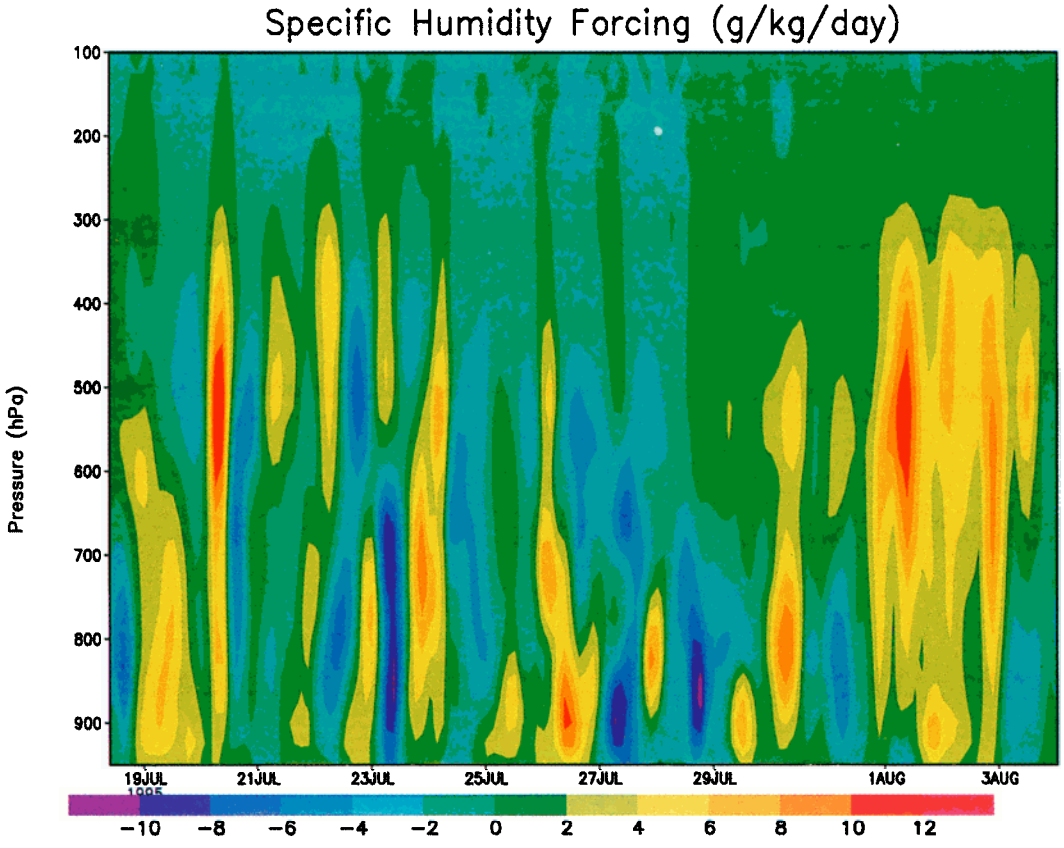


**Plate 2.** As in Plate 1, but the specific humidity forcing (g/kg/d).

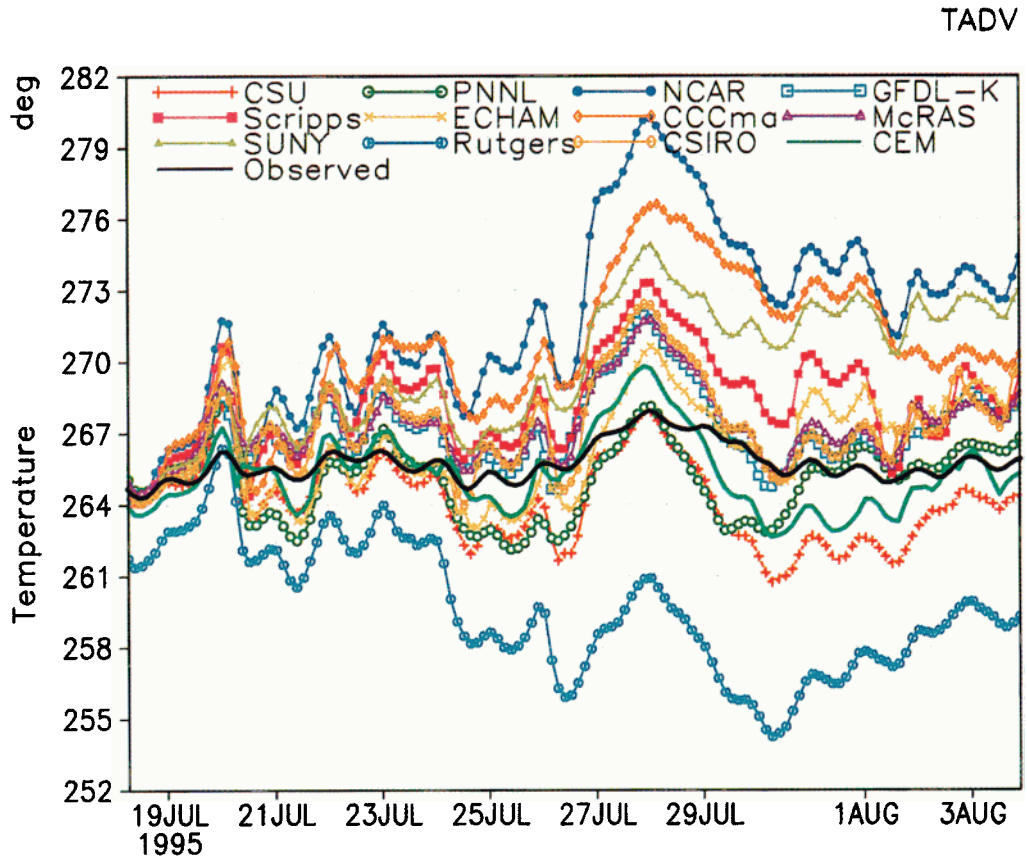


**Plate 3.** Column (100-900 hPa) mean temperature (° Kelvin) as simulated by each model using the baseline forcing shown in Plates 1 and 2, and as observed using the SUNY variational analysis.

observed, particularly on timescales of several days. Because the simulations agree quite well with each other on timescales of less than several days, the greater variability in the simulations is probably due to errors in the forcing on those timescales, which is accentuated in models driven by prescribed vertical velocity or vertical advection because they are unable to disperse heating errors laterally through geostrophic adjustment (of course, all models could have the same problem contributing to the greater variability, but this is unlikely given the variety of parameterizations in the models). Thus by comparing multiple model simulations with each other and with observations, we can separate errors associated with the forcing (on timescales less than a few days) and errors associated with the models (on longer time scales). This illustrates the power of evaluating multiple models in the same study: it would be impossible to separate model and forcing errors from simulations by a single model.

Plate 4 compares the simulated and observed column water vapor (also known as precipitable water). Some of the same features evident in the temperature record also appear in the humidity record, with the simulations agreeing with each other on timescales of less than several days but not on longer timescales. In some cases (NCAR) the simulations that are too warm are also too moist, but in others, the simulations that are too warm are too dry (CCCma) and those that are too cold are too moist (PNNL). Only 3 of the 12 simulations diverge significantly from the observations before 12 days into the experiment. The PNNL simulation is too moist because it neglects subgrid variability in cloud microphysics and hence requires a higher humidity for condensation and precipitation to occur. The ECHAM simulation is too moist because it seldom simulates convective precipitation and hence relies on stratiform condensation to reduce the humidity. The dry and warm bias in the CCCma simulation may be due to insufficient evaporation of rain in the cumulus convection scheme, but further tests are needed to unambiguously identify the cause of the bias. As might be expected, the simulation by the CEM is closest to the temperature and humidity measurements.

How well do the models simulate cloud water? Plate 5 compares the simulated and observed cloud liquid water path (LWP). The observations show a remarkably persistent liquid water path of 0.05-0.2 kg $m^{-2}$ until July 29 (the microwave radiometer was down between July 29 and August 1) and then much larger LWP, 0.2-0.35 kg $m^{-2}$, for the period August 1 – 3. The PNNL model simulates almost no LWP for the entire simulation period. All others simulate LWP sporadically through-

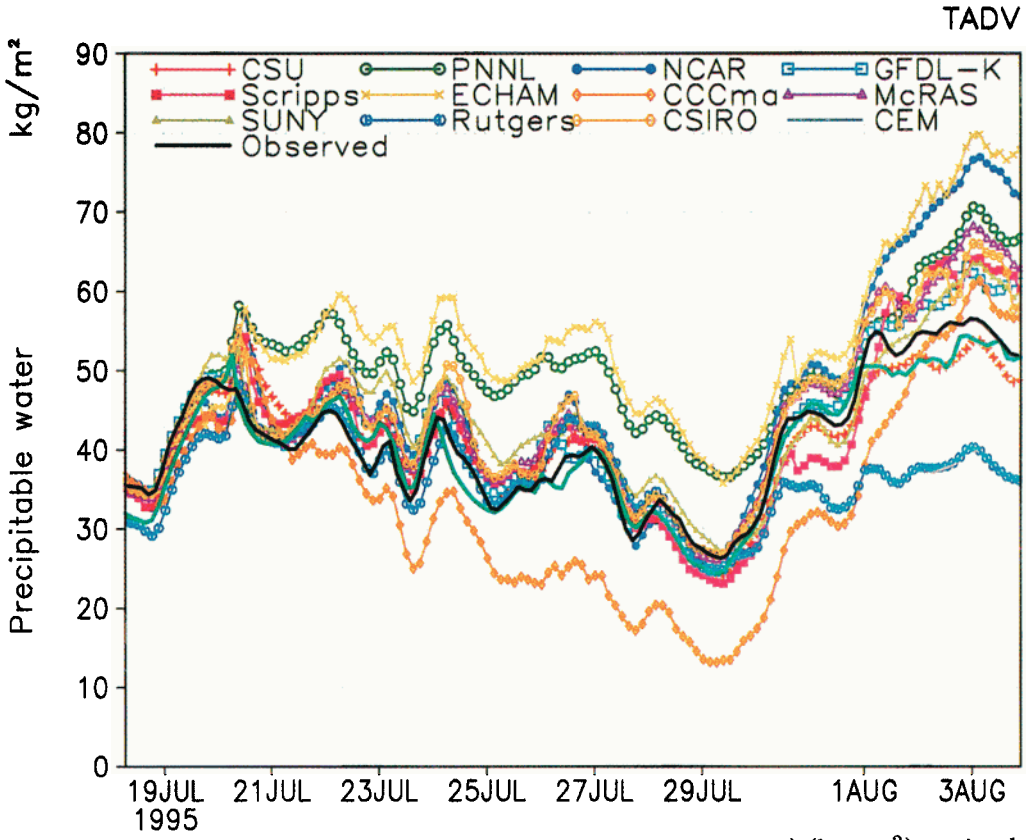


**Plate 4.** Column total water vapor (also known as precipitable water) (kg $m^{-2}$) as simulated by each model using the baseline forcing shown in Plates 1 and 2, and as observed using the SUNY variational analysis.

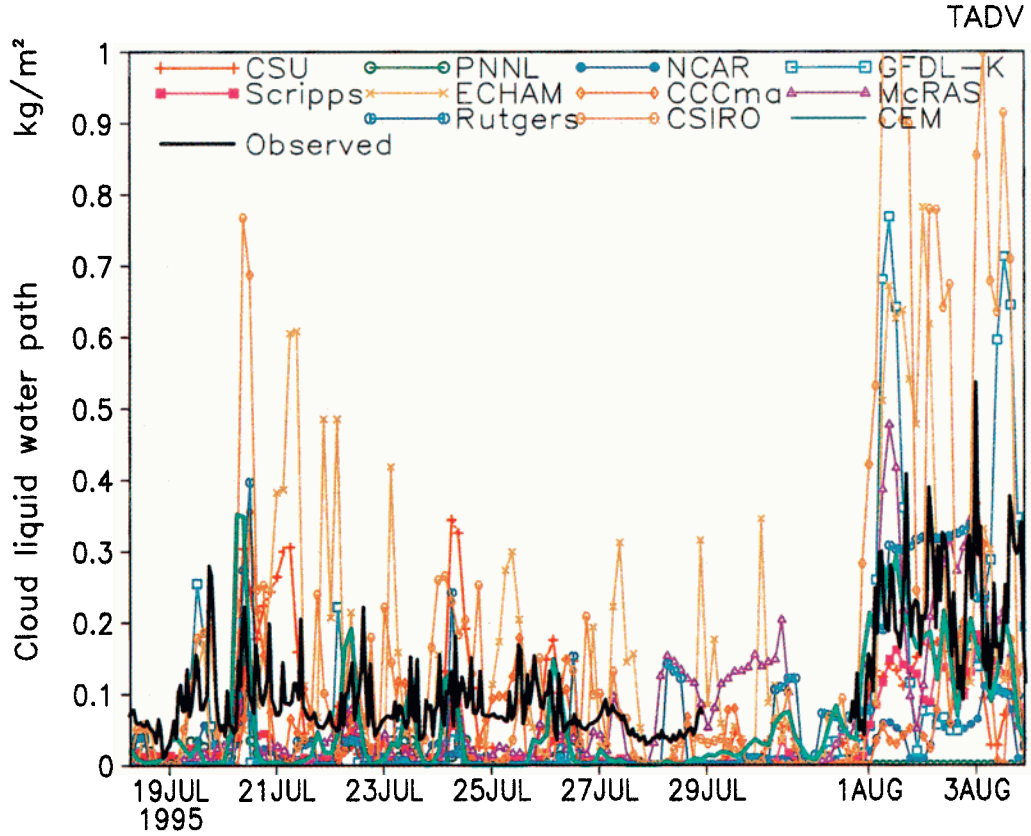


**Plate 5.** Column cloud liquid water (also known as cloud liquid water path) (kg $m^{-2}$) as simulated by each model using the baseline forcing shown in Plates 1 and 2, and as observed by microwave radiometer.

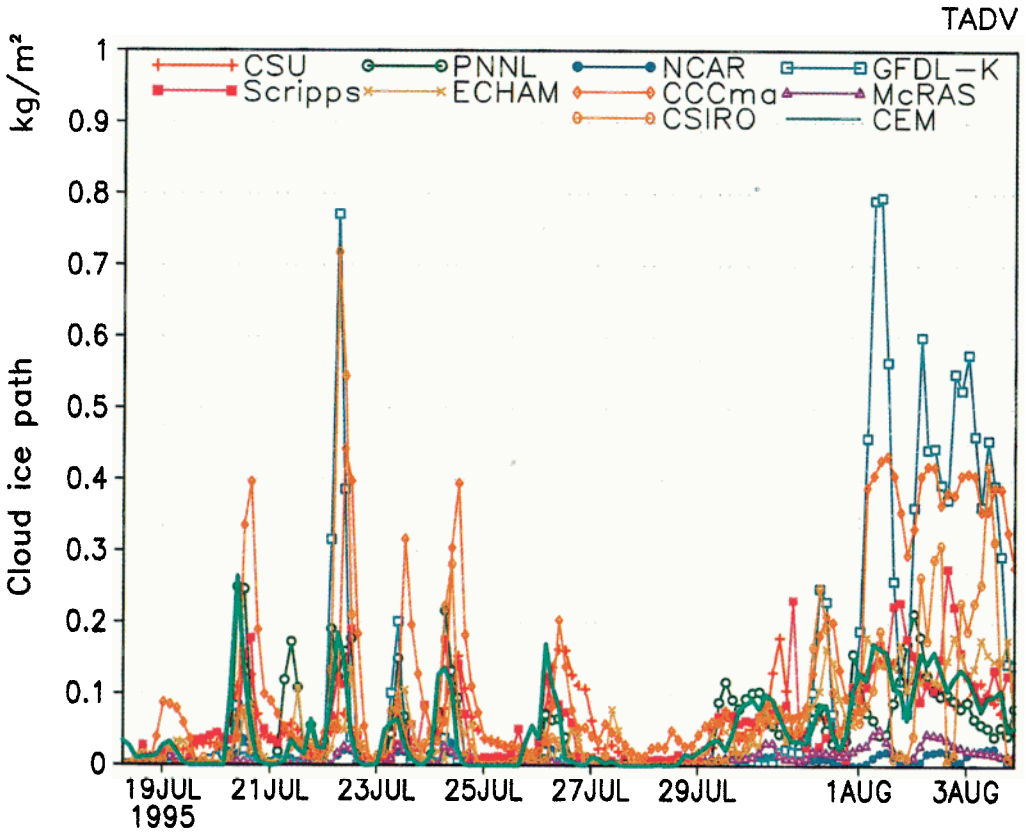


**Plate 6.** Column cloud ice water (also known as cloud ice path) (kg $m^{-2}$) as simulated by each model using the baseline forcing shown in Plates 1 and 2. Observations are not available.

out the simulation period, with intermittent periods of almost no simulated cloud liquid water when the observations indicate liquid water was present. This descrepancy may reflect the excessive variability in the simulated temperature on timescales of less than a few days, which (as discussed above) is likely due to excessive variability in the model forcing. Although the difference could be attributed to the neglect of convective cloud water in several models or to deficiencies in cumulus parameterizations in all SCMs, the fact that the difference is evident in the CEM simulation suggests it is most likely due to the forcing (instrumental error, sampling error, or the lack of any estimate of horizontal advective tendency for cloud water). Insufficient resolution for shallow convection or problems with the treatment of turbulence or cloud microphysics in the CEM could also contribute to the simulation of little LWP by the CEM at times during the period July 19–29. However, a comparison of the observed LWP with surface weather summaries and with satellite estimates of cloud cover indicates sustained periods (e.g., July 27 and 28) when the cloud cover is less than 5%, but the LWP estimated from microwaver radiometer is 0.04 kg $m^{-2}$ (slightly above the estimated uncertainty). Thus the persistence in the observed LWP may not be real.

Plate 6 compares the simulated cloud ice path (IWP). The timing of the ice clouds is generally in good agreement for all models. Observations of IWP are not available. If we can regard the CEM simulation as close to the ice that would be observed, then several of the models (CSU, PNNL, Scripps, ECHAM, CSIRO) simulate the cloud ice fairly well. The model that simulates little liquid water (PNNL) simulates only a moderate amount of ice, suggesting that its problem is due to the fact that it treats only stratiform cloud water, and as we shall see, most of its precipitation is due to convective rather than stratiform clouds.

To some extent the differences in the simulated condensed water can be explained in terms of differences in the treatment of stratiform microphysics, of convective microphysics, or of detrainment of condensate from convective clouds. For example, in the PNNL simulation, convective clouds dominate the precipitation rate and hence control the humidity in the atmosphere, limiting large-scale condensation and hence LWP because convective LWP is neglected. In the ECHAM simulation, stratiform clouds dominate the precipitation rate, so LWP is quite high even though convective LWP is also neglected. The CSIRO model also produces high LWP but for different reasons, namely (1) because its LWP includes convective as well as stratiform LWP, and (2)

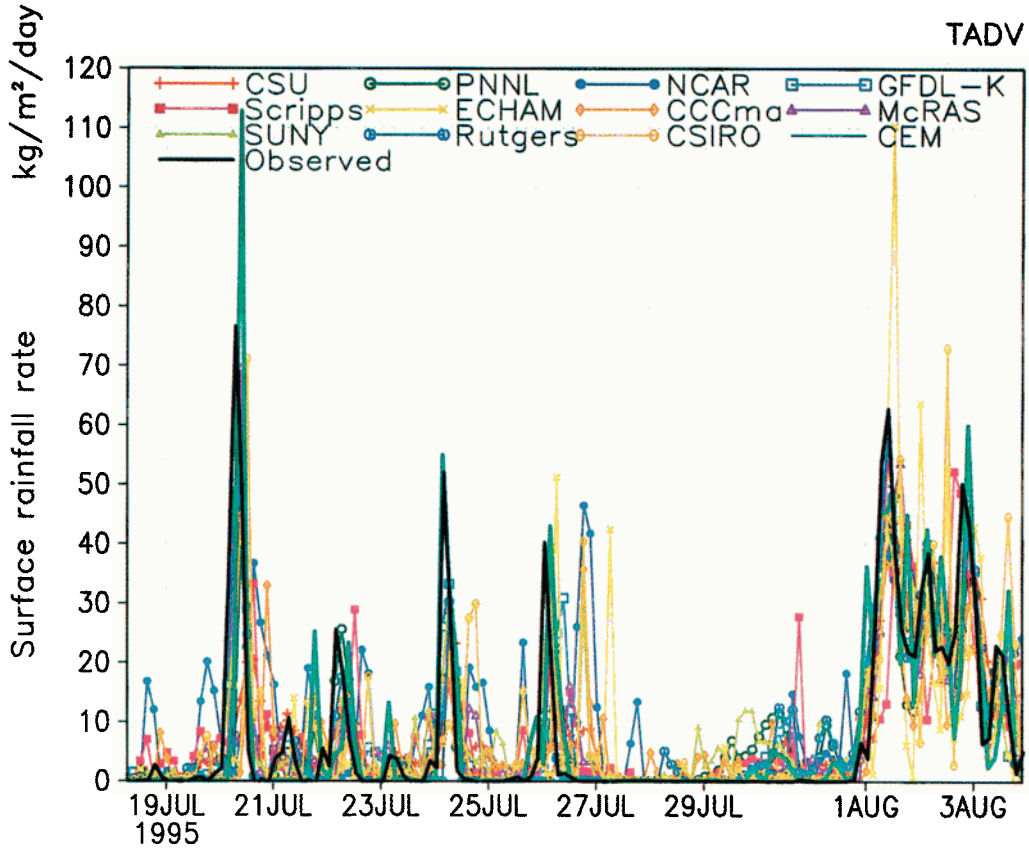


**Plate 7.** Hourly mean surface precipitation rate (kg $m^{-2}$/d) as simulated by each model using the baseline forcing shown in Plates 1 and 2, and as observed.

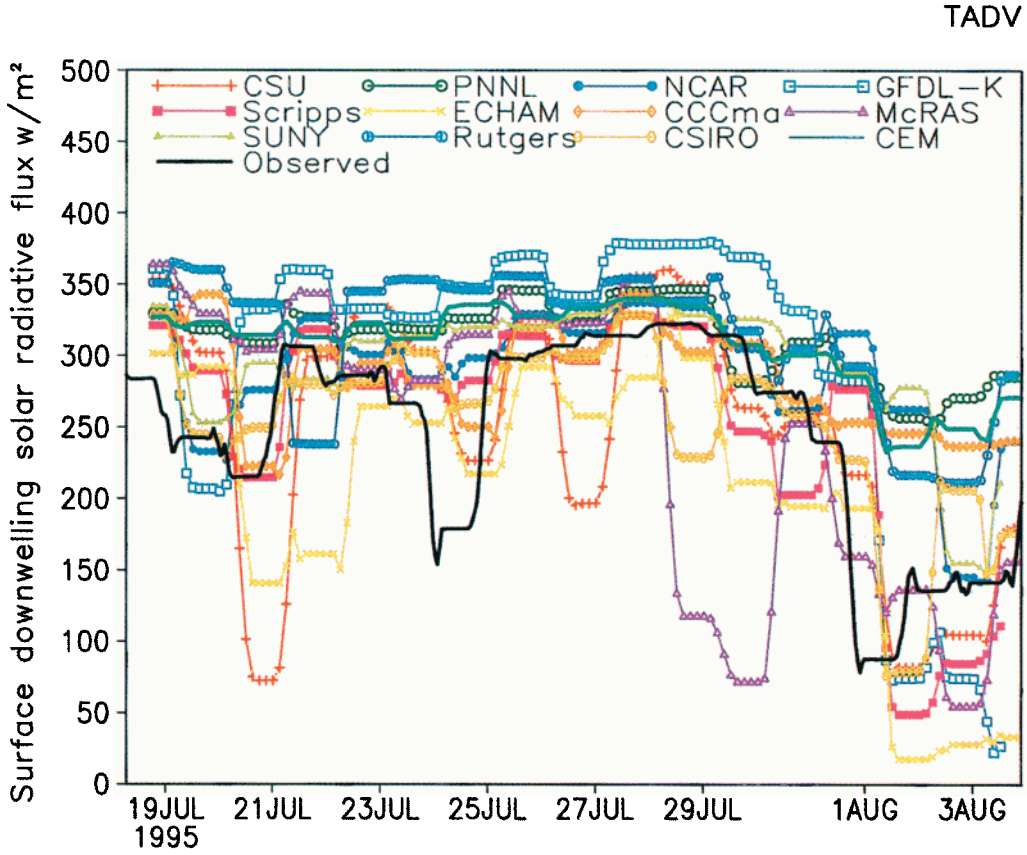


**Plate 8.** Downward 24 hour running mean solar radiative flux at the surface (W $m^{-2}$) as simulated by each model using the baseline forcing shown in Plates 1 and 2, and as observed.

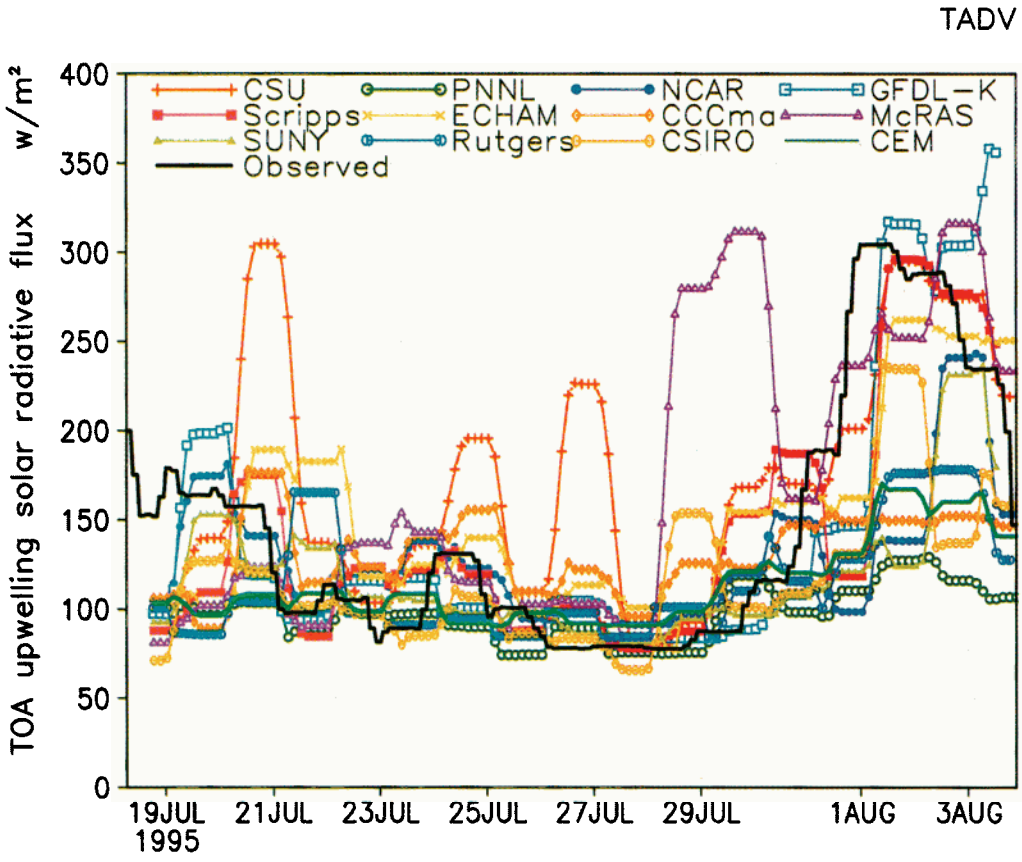


**Plate 9.** Upward 24 hour running mean solar radiative flux at the top of the atmosphere (W $m^{-2}$) as simulated by each model using the baseline forcing shown in Plates 1 and 2, and as observed.

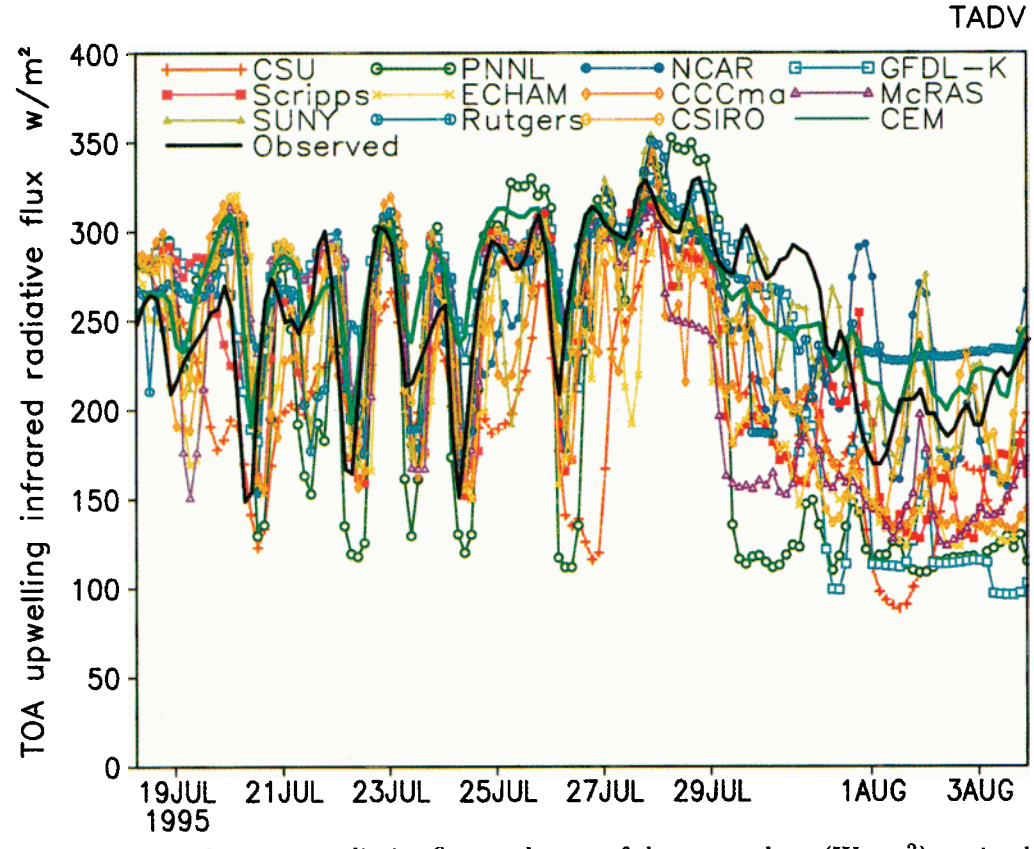


**Plate 10.** Outgoing longwave radiative flux at the top of the atmosphere (W $m^{-2}$) as simulated by each model using the baseline forcing shown in Plates 1 and 2, and as observed.

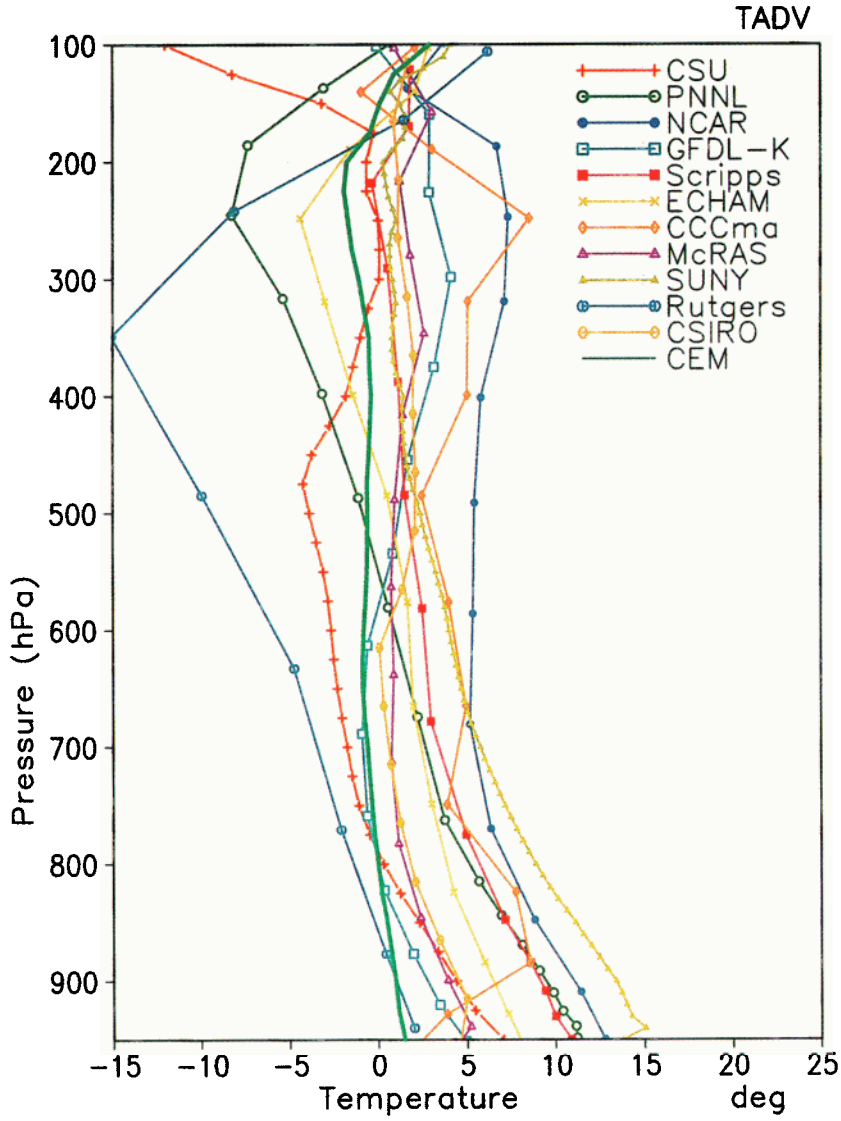


**Plate 11.** Vertical profile of the 17 day mean temperature bias (° Celsius)simulated by each model using the baseline forcing shown in Plates 1 and 2.

because of an oversight in which it neglects cloud water accretion by convective precipitation. Detrainment of condensate from convective clouds may explain why the ECHAM simulation (which treats detrainment) yields more LWP than the CCCma simulation (which neglects it), but the difference in the treatment of droplet number (prescribed versus predicted) could also contribute to the difference. Detrainment does not play so great a role in the McRAS simulation, which yields moderate LWP and little IWP, perhaps because the McRAS model includes convective LWP and IWP. The GFDL SCM simulates the most cloud ice, probably because its cloud ice includes falling snow as well as suspended particles, while other models distinguish between snow and ice. Although the droplet number concentration prescribed or predicted in the SCMs varies from 50 $cm^{-3}$ to 600 $cm^{-3}$ , there is little correlation between droplet number and liquid water path across SCM simulations.

Plate 7 compares observed and simulated precipitation rates at the surface. The agreement is generally quite good, perhaps because the model forcing is constrained by the observed precipitation. Although spurious precipitation is simulated by some models during periods when no precipitation is observed (e.g., July 27–31), all models simulate precipitation to within perhaps 50% of observations during the times when precipitation is observed (July 20, 22, 24, 26, and August 1–3).

The partitioning of the precipitation is quite different for each model. The convective precipitation (not shown) exceeds the stratiform precipitation (not shown) throughout the period for most simulations and dominates in the PNNL and NCAR simulations. On the other hand, stratiform precipitation dominates convective precipitation in the ECHAM simulation throughout the period and in the CCCma simulation during the last week. It is noteworthy that almost all of the

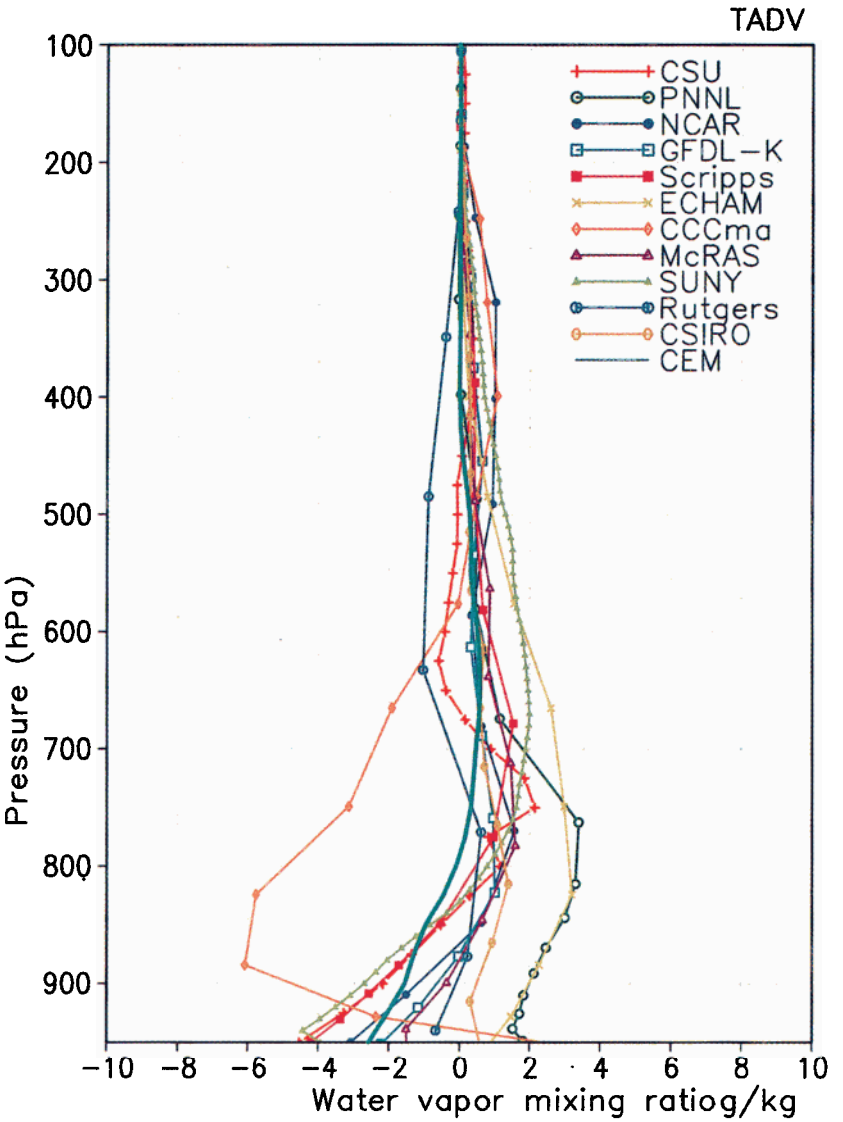


**Plate 12.** Vertical profile of the 17 day mean water vapor mixing ratio bias (g/kg) simulated by each model using the baseline forcing shown in Plates 1 and 2.

spurious precipitation evident in Plate 7 is associated with convective precipitation. Although this suggests that problems with the cumulus parameterizations in the SCM are responsible for the spurious precipitation, the fact that CEM also simulates spurious precipitation at times suggests that errors in the forcing might also be responsible. The excessive cooling during the period July 28–30 simulated by all models (Plate 2) also supports this conclusion.

The radiative flux fields are closely related to the cloud fields. Plate 8 compares the 24-hour running means of the simulated and observed downward solar flux at the surface. The observed flux is typically 250–320 W $m^{-2}$, except during the disturbed period August 1–3, when it is 100–150 W $m^{-2}$. Although some simulations follow this general pattern, most models produce large errors at times. The flux simulated by the CSU, McRAS, and ECHAM models is frequently 100 W $m^{-2}$ too low during July, reflecting the excessive cloud water evident in Plate 5. The flux simulated by the PNNL, CCCma, Rutgers, and CEM is 10–150 W $m^{-2}$ too high on August 1–3. The overestimate of the flux by the PNNL model during the disturbed period is likely due to its neglect of the radiative impact of convective clouds. The overestimate of the flux by the CCCma is a problem with particle phase because it simulates too much cloud ice (which is less efficient at scattering sunlight) and too little cloud liquid water. The overestimate of the flux by the Rutgers SCM and the CEM must be due to improper cloud particle properties because both models simulate plenty of cloud liquid water and cloud ice. The most accurate flux is

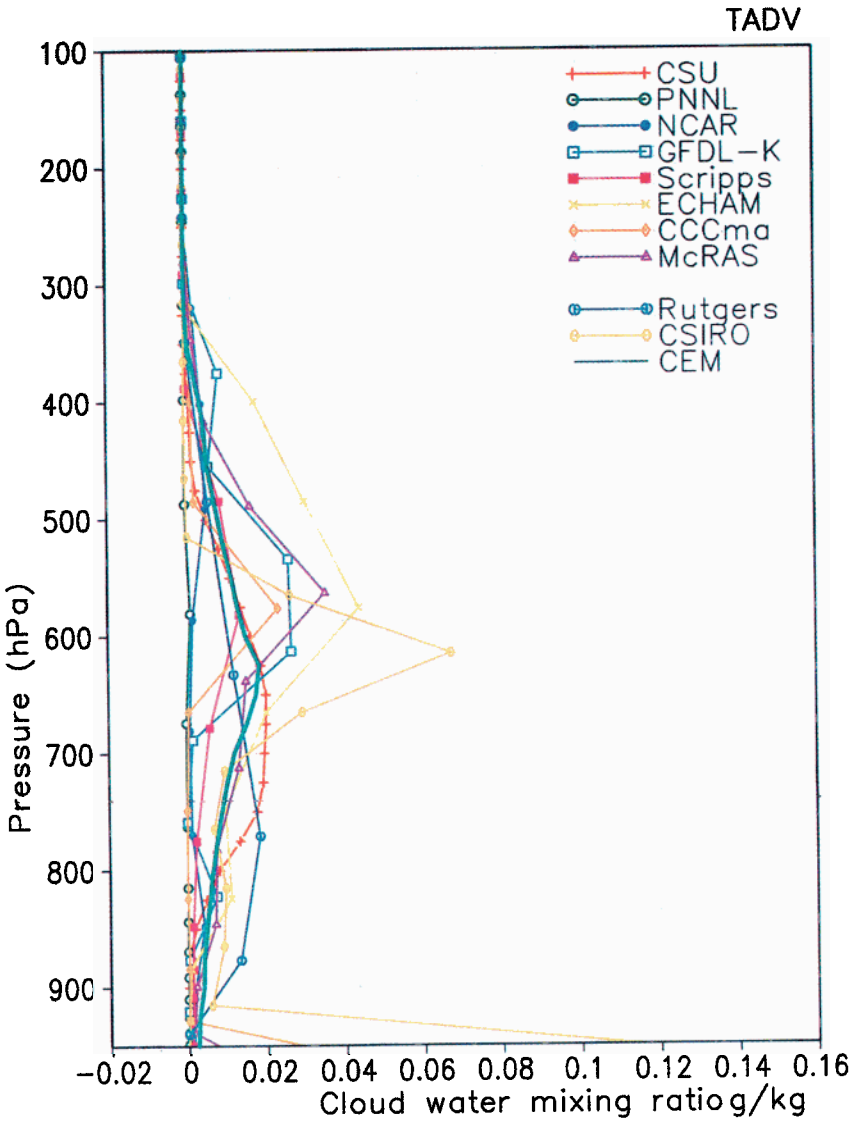


**Plate 13.** Vertical profile of the 17 day mean cloud water mixing ratio (g/kg) simulated by each model using the baseline forcing shown in Plates 1 and 2.

simulated by the CSIRO SCM, even though it predicts far too much cloud liquid water, and by the Scripps SCM.

The features of the downward solar flux at the surface are mirrored in the features of the upward solar flux at the top of the atmosphere. Plate 9 compares 24 hour running means of the simulated and observed upward solar flux at the top of the atmosphere. The observed flux ranges from a low of 80 W $m^{-2}$ July 26-29, to a high of 300 W $m^{-2}$ on August 2. Most models simulate the low outgoing solar radiation quite well, although the CSU and McRAS simulations yield excessively high upward solar flux at times. On the days with high observed outgoing solar radiation the Scripps, CSU, GFDL, and ECHAM simulations are within about 50 W $m^{-2}$ of observations, but the CEM, SUNY, CCCma, and particularly the PNNL simulations are 120–180 W $m^{-2}$ too low. The PNNL bias is due to its neglect of convective cloud radiative effects. The CCCma bias is due to the partitioning of liquid water and cloud ice as discussed above. The CEM bias must be due to inappropriate cloud particle properties because the CEM simulates plenty of cloud water and cloud ice. The solar radiation absorbed in the atmosphere (not shown) by the ECHAM model is up to 100 W $m^{-2}$ higher than any other model; this heating is associated with the presence of upper tropospheric ice clouds and is due to the use of only two solar bands for the radiative transfer.

The outgoing longwave radiative flux at the top of the atmosphere provides information about cloud top temperature as well as cloud water concentration. Plate 10

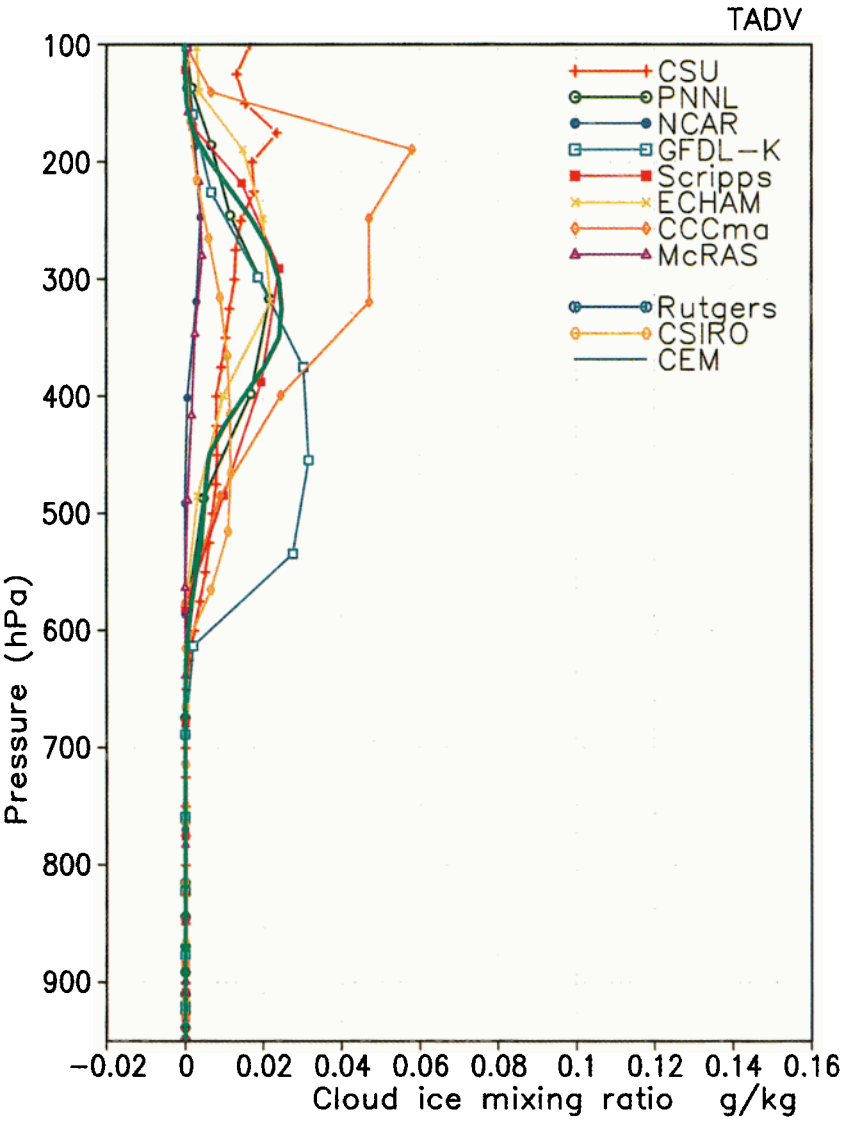


**Plate 14.** Vertical profile of the 17 day mean cloud ice mixing ratio (g/kg) simulated by each model using the baseline forcing shown in Plates 1 and 2.

compares the simulated and observed upward infrared flux at the top of the atmosphere. The observations show considerable temporal variability as high-cloud systems pass across the SGP site, with the outgoing infrared flux varying by up to 150 W $m^{-2}$ from day to day. Most simulations capture this variability quite well, particularly during the period July 22– 26. However, on some days, many of the models tend to simulate spurious high cloud (low upward infrared flux), particularly on July 29 to August 3. Only the SUNY, Rutgers, CEM, and to a lesser extent, the NCAR and CSIRO models seem to avoid this problem. The defect is particularly severe in the PNNL simulation but is also evident in the simulations by the other models that neglect the radiative impact of convective clouds (CSU, CCCma, GFDL, and ECHAM).

To see the vertical structure of the simulations, we now consider vertical profiles of the time means of several variables. Plate 11 compares the vertical profile of the simulated temperature bias averaged over the 17 days of the IOP. The CEM temperature profile agrees with the observations remarkably well, with differences of less than 3°throughout the troposphere. Most SCM simulations are too warm throughout the troposphere, with the greatest warm bias (up to 15° C) in the lower troposphere. The large difference between the NCAR and the SUNY temperature bias (7°in the upper troposphere) is only due to the difference in the triggering function for convection, which is triggered less frequently in the SUNY simulation, producing less warming than in the NCAR simulation. The 15° C upper tropospheric cold bias in the Rutgers simulation is due to the Rutgers moist convection scheme, which diffuses moist static energy only under conditions of instability and saturation [*Stenchikov and Robock,* 1995]; although the atmosphere is always unstable in the Rutgers simu-

**Table 10.** Time and Column Mean Temperature (° Kelvin) Between 100 and 900 hPa

| Model | Baseline | LLNL | EBBR | Nudging | VADV |
|---|---|---|---|---|---|
| Observed | 265.8 | | | | |
| CCCma SCM | 270.4 | 271.4 | 270.6 | 266.2 | 270.3 |
| CSIRO SCM | 267.3 | 265.8 | 266.9 | 265.6 | 265.2 |
| CSU SCM | 264.1 | 264.9 | 265.1 | 266.4 | 266.3 |
| ECHAM SCM | 266.4 | 266.5 | 266.2 | 265.4 | 267.3 |
| GFDL SCM | 267.1 | 265.9 | 267.2 | 265.5 | 268.4 |
| McRAS SCM | 267.3 | 265.7 | 267.3 | 265.7 | 269.0 |
| NCAR CCM3 SCM | 271.8 | 274.8 | 273.0 | 265.9 | 274.0 |
| PNNL/CCM2 SCM | 265.0 | 264.8 | 264.7 | 265.3 | 267.5 |
| Rutgers SCM | 259.7 | 266.8 | 260.0 | 264.0 | 261.0 |
| Scripps SCM | 268.3 | 269.2 | 268.1 | 265.6 | 271.4 |
| SUNY/CCM3 SCM | 269.7 | 274.5 | 270.0 | 265.9 | 270.4 |
| UCLA/CSU CEM | 265.3 | | 265.8 | | 266.7 |

lation, it is seldom saturated, and when it is the moist convection scheme does not eliminate the instability.

Plate 12 shows the vertical profile of the simulated bias in the water vapor mixing ratio. Most model simulations are too moist between 700 and 800 hPa and too dry below 900 hPa. In contrast, the CCCma simulation is far too dry throughout the lower troposphere, which is consistent with the low precipitable water in the CCCma simulation; this dryness, coupled with the warm bias, suggests that evaporation of precipitation is too weak in the CCCma simulation. The PNNL simulation is too moist at all levels because it neglects subgrid variability in cloud microphysics and hence requires a higher humidity for condensation and precipitation to occur. The ECHAM simulation is too moist at all levels because it seldom simulates convective precipitation and hence relies on stratiform condensation to reduce the humidity. The CEM simulation is too dry near the surface.

The simulated vertical profiles of average cloud water and cloud ice mixing ratios are illustrated in Plates 13 and 14. The CSIRO model simulates cloud liquid water (nocturnal fog) near the surface. Most models (except PNNL) simulate cloud liquid water at levels 500–800 hPa. The Rutgers model simulates most of its liquid water at lower levels than most models, while the NCAR model simulates most of its liquid water at higher levels than most models; interestingly, both of these models prescribe rather than predict the cloud liquid water profile. Most models simulate most cloud ice at levels above 400 hPa, but the CSIRO and the GFDL-K models simulate most cloud ice below 400 hPa because the diagnostic for cloud ice in both the CSIRO and GFDL models includes the precipitating particles (loosely, snow and graupel) which are added back into the cloud ice field in the layer in which they arrive at the end of each time step. The NCAR and McRAS models simulate very little cloud ice at any level, while the CCCma model simulates much more cloud ice than the other models, even though it does not treat detrainment of condensed water from convective clouds.

Tables 10- 17 summarize the baseline and other simulations with time means of column-integrated fields. The time mean values are consistent with the above

**Table 11.** Time Mean Column Water Vapor (kg $m^{-2}$)

| Model | Baseline | LLNL | EBBR | Nudging | VADV |
|---|---|---|---|---|---|
| Observed | 41.1 | | | | |
| CCCma SCM | 34.0 | 29.2 | 34.8 | 39.5 | 33.1 |
| CSIRO SCM | 44.7 | 29.7 | 45.3 | 41.6 | 39.6 |
| CSU SCM | 41.4 | 29.3 | 43.7 | 41.8 | 45.2 |
| ECHAM SCM | 53.4 | 34.1 | 54.3 | 43.7 | 55.7 |
| GFDL SCM | 43.1 | 28.3 | 44.1 | 41.1 | 45.3 |
| McRAS SCM | 44.6 | 34.0 | 43.4 | 37.5 | 37.6 |
| NCAR CCM3 SCM | 46.2 | 33.0 | 47.7 | 41.0 | 49.6 |
| PNNL/CCM2 SCM | 50.5 | 38.9 | 51.8 | 43.1 | 60.2 |
| Rutgers SCM | 36.8 | 22.7 | 37.5 | 36.5 | 40.0 |
| Scripps SCM | 42.2 | 30.6 | 44.1 | 41.0 | 50.3 |
| SUNY/CCM3 SCM | 44.2 | 33.7 | 44.4 | 41.0 | 46.6 |
| UCLA/CSU CEM | 40.4 | | 42.4 | | 43.9 |

**Table 12.** Time Mean Column Cloud Liquid Water (kg $m^{-2}$)

| Model | Baseline | LLNL | EBBR | Nudging | VADV |
|---|---|---|---|---|---|
| Observed | 0.111 | | | | |
| CCCma SCM | 0.041 | 0.031 | 0.038 | 0.019 | 0.039 |
| CSIRO SCM | 0.187 | 0.133 | 0.228 | 0.127 | 0.175 |
| CSU SCM | 0.060 | 0.028 | 0.071 | 0.019 | 0.062 |
| ECHAM SCM | 0.138 | 0.076 | 0.114 | 0.087 | 0.177 |
| GFDL SCM | 0.065 | 0.054 | 0.054 | 0.042 | 0.046 |
| McRAS SCM | 0.078 | 0.058 | 0.065 | 0.007 | 0.019 |
| NCAR CCM3 SCM | 0.018 | 0.009 | 0.023 | 0.022 | 0.014 |
| PNNL/CCM2 SCM | 0.006 | 0.041 | 0.003 | 0.011 | 0.030 |
| Rutgers SCM | 0.063 | 0.043 | 0.071 | 0.047 | 0.081 |
| Scripps SCM | 0.035 | 0.025 | 0.035 | 0.029 | 0.034 |
| SUNY/CCM3 SCM | - | - | - | - | - |
| UCLA/CSU CEM | 0.058 | | 0.052 | | 0.065 |

discussion. These values are presented for comparison with time mean values for sensitivity experiments described in section 5.

## 5. Comparison of Forcing Methods

In designing this comparison experiment we had to choose from among several different forcing methods. To determine the dependence of the results on this choice, here we investigate the sensitivity of the simulations to the choice of forcing methods. In particular, we examine the sensitivity to (1) the analysis method (LLNL versus SUNY), (2) the prescribed surface fluxes (EBBR versus SiB), (3) the nudging of temperature and humidity, and (4) whether the vertical advective tendencies of temperature and humidity are prescribed from the analysis or calculated by each model from the simulated profiles of temperature/humidity and the analyzed vertical velocity.

### 5.1. LLNL versus SUNY Forcing

Figure 2 shows the 18 day mean and standard deviation of the temperature and specific humidity total advective tendencies as analyzed at LLNL and at SUNY. The temperature tendency shows good agreement between the two analyses except for 2°/d less cooling between 850 and 375 hPa in the LLNL analysis. The moisture tendency of the LLNL analysis shows much larger temporal variations and noticeably more complicated vertical structures in both the mean and the standard deviation profiles, with less moistening and more drying in the lower troposphere. This could impact the simulated results.

The most important difference between the LLNL and the SUNY objective analyses is the added constraint of column heat and moisture consistency in the SUNY objective analysis. Figure 3 shows the column moisture budget for the SUNY and LLNL analyses, expressed in terms of the precipitation rate and the sum of the surface evapotranspiration rate and the column integral of the apparent moisture sink $Q_2$ [*Yanai et al.*, 1973]. The apparent moisture sink is determined from the analyzed difference between the total tendency and the advective tendency of moisture. Although the SUNY analysis ensures an exact column moisture balance when the advective tendency is expressed in its flux form

**Table 13.** Time Mean Column Cloud Ice (kg $m^{-2}$)

| Model | Baseline | LLNL | EBBR | Nudging | VADV |
|---|---|---|---|---|---|
| CCCma SCM | 0.130 | 0.099 | 0.121 | 0.112 | 0.136 |
| CSIRO SCM | 0.062 | 0.045 | 0.065 | 0.059 | 0.086 |
| CSU SCM | 0.058 | 0.052 | 0.046 | 0.026 | 0.052 |
| ECHAM SCM | 0.051 | 0.035 | 0.051 | 0.011 | 0.054 |
| GFDL SCM | 0.096 | 0.077 | 0.101 | 0.052 | 0.085 |
| McRAS SCM | 0.010 | 0.015 | 0.009 | 0.000 | 0.002 |
| NCAR CCM3 SCM | 0.007 | 0.003 | 0.006 | 0.005 | 0.008 |
| PNNL/CCM2 SCM | 0.050 | 0.041 | 0.051 | 0.065 | 0.064 |
| Rutgers SCM | - | - | - | - | - |
| Scripps SCM | 0.061 | 0.040 | 0.055 | 0.039 | 0.048 |
| SUNY/CCM3 SCM | - | - | - | - | - |
| UCLA/CSU CEM | 0.051 | | 0.053 | | 0.046 |

**Table 14.** Time Mean Precipitation Rate (kg $m^{-2}$ $d^{-1}$)

| Model | Baseline | LLNL | EBBR | Nudging | VADV |
|---|---|---|---|---|---|
| Observed | 7.81 | | | | |
| CCCma SCM | 6.49 | 5.19 | 5.60 | 8.37 | 4.61 |
| CSIRO SCM | 7.91 | 4.76 | 7.96 | 6.69 | 6.62 |
| CSU SCM | 8.17 | 4.42 | 8.06 | 5.01 | 8.55 |
| ECHAM SCM | 5.96 | 3.57 | 5.39 | 0.41 | 7.63 |
| GFDL SCM | 7.68 | 4.45 | 7.76 | 8.16 | 9.01 |
| McRAS SCM | 7.87 | 4.77 | 7.99 | 0.40 | 2.99 |
| NCAR CCM3 SCM | 9.88 | 8.11 | 10.24 | 14.4 | 11.53 |
| PNNL/CCM2 SCM | 7.33 | 5.44 | 7.23 | 4.39 | 8.82 |
| Rutgers SCM | 6.97 | 4.30 | 7.27 | 1.80 | 2.36 |
| Scripps SCM | 7.98 | 5.96 | 8.12 | 7.71 | 9.01 |
| SUNY/CCM3 SCM | 9.13 | 7.34 | 9.01 | 10.0 | 9.71 |
| UCLA/CSU CEM | 8.19 | | 9.01 | | 9.17 |

$$\left(\frac{\partial \bar{q}}{\partial t}\right)_{\text{L.S.}} \equiv -\left(\nabla \cdot \bar{q}\bar{\mathbf{v}} + \frac{\partial \bar{q}\bar{\omega}}{\partial p}\right), \qquad (8)$$

it does not guarantee an exact balance for the advective form (which is used to drive the models); the same holds for the advective tendency of heat. In addition, there was an inconsistency in the use of the surface $\omega$ in the SUNY analysis. Thus in the SUNY analysis the precipitation rate differs from the sum of the evapotranspiration rate and the advective form of the apparent moisture sink by typically 100 $Wm^{-2}$ with a mean difference of 10 $Wm^{-2}$ of excessive advective moistening . Zhang has recently revised the diagnostic calculation of the advective form to preserve the exact column balance of heat and moisture. Most of the SCM simulations of the July 1995 IOP using the revised SUNY analysis are 1 °–2 ° deg cooler and 10% drier than simulations using the uncorrected analysis. The impact of the correction on the simulated clouds and precipitation is small because the effects of cooling and drying on relative humidity largely cancel. The revised (energy- and moisture-conserving) analysis will be applied to all subsequent ARM IOPs, starting with the July 1997 IOP. The column moisture imbalance in the LLNL analysis, on the other hand, is much larger, with an imbalance of typically 300–600 $Wm^{-2}$ and a mean difference of 75 $Wm^{-2}$.

The improved consistency in the heat and moisture budgets of the SUNY analysis is enough to clearly identify it as the preferred analysis scheme. However, the SUNY analysis scheme cannot be applied anywhere because it requires measurements of the surface heat, moisture and radiative fluxes. To better appreciate the value of the SUNY analysis, the SCMs have been run using the LLNL analysis. As might be expected, the response of the models to the warming and drying in the forcing is generally a warmer and drier simulation. Tables 10–17 list the time means of column integrated and single-level fields simulated by each model driven by the LLNL forcing. Comparing the column mean temperature simulated with LLNL and SUNY forcing, three of the models (NCAR, SUNY, and Rutgers) produced a much warmer (about 5° C) simulation when driven by the LLNL forcing compared with SUNY forcing, while the others were relatively insensitive not only in the column mean but also at each level. The column water vapor, on the other hand, is sensitive to the forcing for all models, with reductions of at least 10 kg $m^{-2}$ for almost every model. The warming and drying reduced the cloud liquid water for every model except PNNL,

**Table 15.** Time Mean Downward Shortwave Radiation at the Surface (W $m^{-2}$)

| Model | Baseline | LLNL | EBBR | Nudging | VADV |
|---|---|---|---|---|---|
| Observed | 246 | | | | |
| CCCma SCM | 288 | 302 | 302 | 298 | 301 |
| CSIRO SCM | 257 | 287 | 257 | 290 | 263 |
| CSU SCM | 250 | 281 | 248 | 308 | 241 |
| ECHAM SCM | 204 | 229 | 192 | 259 | 185 |
| GFDL SCM | 292 | 289 | 302 | 323 | 296 |
| McRAS SCM | 248 | 239 | 267 | 348 | 330 |
| NCAR CCM3 SCM | 290 | 319 | 284 | 297 | 292 |
| PNNL/CCM2 SCM | 314 | 280 | 312 | 312 | 286 |
| Rutgers SCM | 317 | 331 | 321 | 316 | 285 |
| Scripps SCM | 252 | 276 | 258 | 274 | 256 |
| SUNY/CCM3 SCM | 298 | 328 | 294 | 294 | 297 |
| UCLA/CSU CEM | 310 | | 315 | | 313 |

**Table 16.** Time Mean Upward Shortwave Radiation at Top of Atmosphere (W $m^{-2}$)

| Model | Baseline | LLNL | EBBR | Nudging | VADV |
|---|---|---|---|---|---|
| Observed | 145 | | | | |
| CCCma SCM | 133 | 115 | 123 | 123 | 124 |
| CSIRO SCM | 117 | 99 | 116 | 94 | 114 |
| CSU SCM | 175 | 152 | 175 | 127 | 181 |
| ECHAM SCM | 155 | 142 | 158 | 119 | 166 |
| GFDL SCM | 150 | 149 | 143 | 126 | 144 |
| McRAS SCM | 170 | 176 | 155 | 88 | 104 |
| NCAR CCM3 SCM | 129 | 108 | 132 | 122 | 129 |
| PNNL/CCM2 SCM | 99 | 125 | 99 | 104 | 119 |
| Rutgers SCM | 115 | 109 | 111 | 113 | 136 |
| Scripps SCM | 146 | 124 | 137 | 122 | 140 |
| SUNY/CCM3 SCM | 120 | 94 | 121 | 122 | 121 |
| UCLA/CSU CEM | 115 | | 111 | | 113 |

which actually simulated much more cloud liquid water because of an increase in water vapor during the period August 1–3. Cloud ice is also less with LLNL forcing for most models. Precipitation is therefore greatly reduced in all simulations, primarily due to inadequate precipitation during the periodic precipitation events July 20–27. Downward solar at the surface is increased, upward solar at the top of the atmosphere is reduced, and upward longwave radiation is increased in almost all simulations. In most cases the changes in the simulations with LLNL forcing are for the worse when compared with observations. This was one of the main reasons for adopting the SUNY forcing data in this study.

### 5.2. SiB2 vs EBBR Fluxes

The importance of the surface fluxes in initializing cumulus convection over land is easy to understand, but the impact of surface fluxes on the intensity of cumulus convection has not received much attention. The SiB-derived surface sensible and latent heat fluxes are very different in magnitude from the EBBR fluxes [see *Doran et al.*, 1998] because of the limited sampling of vegetation types by the 10 EBBR stations. The SiB-derived sensible heat fluxes are twice as large as the EBBR fluxes during daytime of dry subperiods and larger by about 100 W $m^{-2}$ during daytime of other subperiods. The SiB-derived latent heat fluxes are smaller by 100 W $m^{-2}$ during daytime of most subperiods. Such large differences in surface fluxes impact the large-scale advective tendencies estimated by the SUNY variational analysis, but the root-mean-square (rms) differences between the SUNY analyses with Sib and EBBR surface fluxes are only about 1° $d^{-1}$ and 0.3 g $kg^{-1}$ $d^{-1}$ for the advective tendencies of temperature and humidity, respectively. Such differences are much smaller than the rms differences between the LLNL and the SUNY forcings.

However, even if the SUNY analysis were the same for SiB2 and EBBR surface fluxes, simulations using the SiB2 and EBBR fluxes could be quite different because of the large differences in the surface fluxes applied as a lower boundary condition in the simulations. The formulation of the planetary boundary layer (PBL) and the interaction with cumulus convection in SCMs are the most important factors in determining the sensitivity. To address this sensitivity, experiment

**Table 17.** Time Mean Upward Longwave Radiation at Top of Atmosphere (W $m^{-2}$)

| Model | Baseline | LLNL | EBBR | Nudging | VADV |
|---|---|---|---|---|---|
| Observed | 252 | | | | |
| CCCma SCM | 219 | 249 | 227 | 237 | 227 |
| CSIRO SCM | 241 | 264 | 244 | 260 | 236 |
| CSU SCM | 199 | 235 | 212 | 236 | 205 |
| ECHAM SCM | 212 | 231 | 210 | 261 | 205 |
| GFDL SCM | 240 | 254 | 239 | 254 | 245 |
| McRAS SCM | 225 | 212 | 234 | 284 | 273 |
| NCAR CCM3 SCM | 245 | 281 | 254 | 263 | 251 |
| PNNL/CCM2 SCM | 210 | 242 | 214 | 256 | 193 |
| Rutgers SCM | 258 | 278 | 257 | 271 | 250 |
| Scripps SCM | 229 | 264 | 236 | 261 | 242 |
| SUNY/CCM3 SCM | 249 | 297 | 251 | 247 | 246 |
| UCLA/CSU CEM | 262 | | 264 | | 266 |

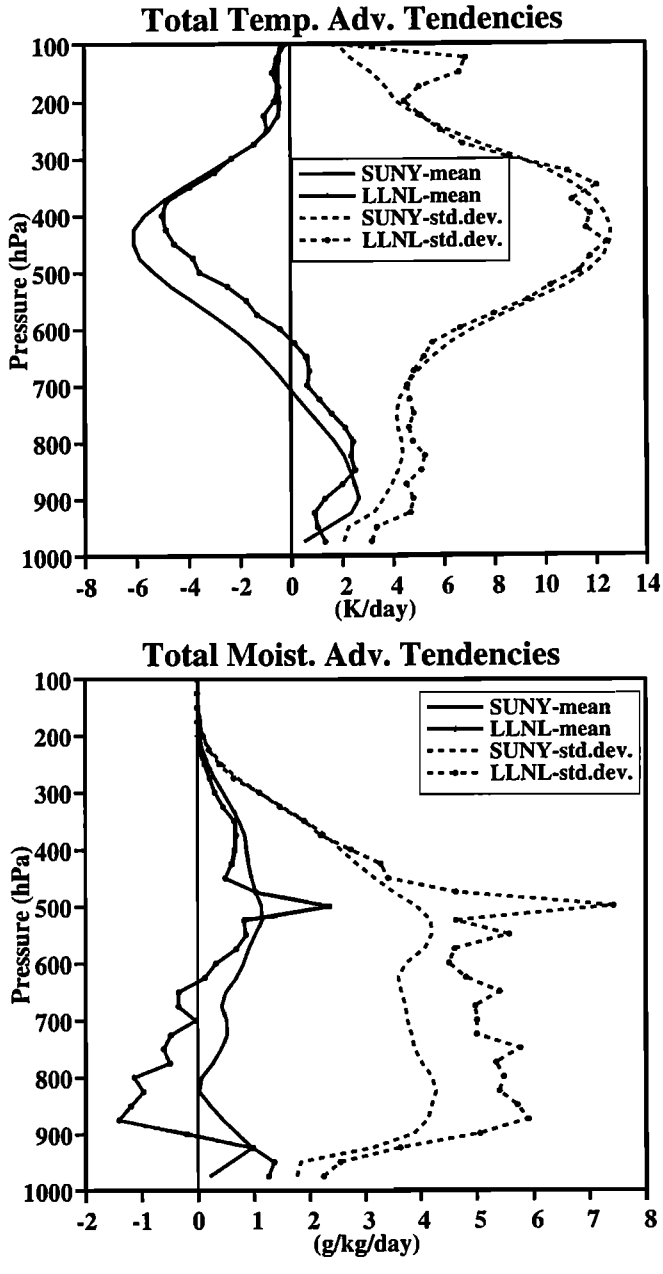


**Figure 2.** Vertical profile of the 17 day mean and standard deviation of the temperature forcing (a) and moisture forcing (b) as analyzed by the SUNY variational analysis and by the LLNL objective analysis.

EBBR uses the EBBR measurements of the mean surface fluxes both as the lower boundary condition for the models and (for consistency) in the SUNY objective analysis. Although the poor representativeness of the EBBR measurements raises questions about the validity of such an experiment, the large differences between the Sib and the EBBR estimates of surface fluxes provide the opportunity to determine the sensitivity of the simulations to larger uncertainties in the surface fluxes. Surprisingly, all models show rather weak sensitivities (compared to the observed variability) or no sensitivity at all in the 18 day mean soundings or the time series of the column mean temperature and specific humidity. The 18-day mean temperature and specific humidity profiles show 1–2 K cooler and 1 g $kg^{-1}$ moister in the lower troposphere with the EBBR fluxes for all models except for Rutgers, CCCma, and ECHAM. The mean temperature for ECHAM is 1 K warmer with the EBBR fluxes. The difference in the mean specific humidity is rather small for ECHAM, CCCma, and McRAS. In all models (except for PNNL) with some sensitivity mentioned above, the 18 day mean temperature differences between the simulations reverse signs near the midtroposphere, between 700 and 500 hPa. This result suggests that the differences in the large-scale advective forcings between the two versions of the SUNY analyses also have some impacts.

Sensitivity of the simulated PBL depth is apparent in some models. With the EBBR fluxes, the amplitude of the diurnal variations of the PBL depths is reduced in the CEM, CSU, and Scripps SCMs (the PBL data were not available for other models), which would impact the initiation of deep convection at the diurnal timescale.

### 5.3. Sensitivity to Nudging

For the baseline simulation we chose not to use nudging for several reasons. First, it simplifies the interpretation of the results because all models are subject to the same advective tendencies. Second, it is more likely to reveal problems in the forcing or in the model physics. However, simulations without nudging are more likely to exhibit sensitive dependence on initial conditions [*Hack and Pedretti,* 1999] and, as discussed in section 5.1, to drift far from the observed state because of errors in forcing.

Here we explore the value of nudging by introducing it in SCM simulations. We nudge both temperature and specific humidity toward the analyzed values for the SGP site. In addition to nudging, the total advective tendency is prescribed as in the baseline simulation. Thus the only difference between this experiment and the baseline experiment is the nudging toward the analysis.

Application of nudging improves most simulations in several respects but degrades some simulations in other respects. In addition to improving the simulated temperature and humidity, nudging improves the simulated cloud and radiation fields. The simulated cloud liquid water path is substantially reduced by nudging, compared to the baseline experiment, for some models, most noticeably McRAS and ECHAM and to a lesser extent most of the other models. This response is primarily due to the moist bias in most models without nudging, so nudging removes water and hence reduces cloud water. Most simulations now underestimate the cloud liquid water path, and only the CSIRO model overestimates it. Although nudging of temperature also cools most simulations, which would increase cloud water, the largest warm biases are in the models that prescribe

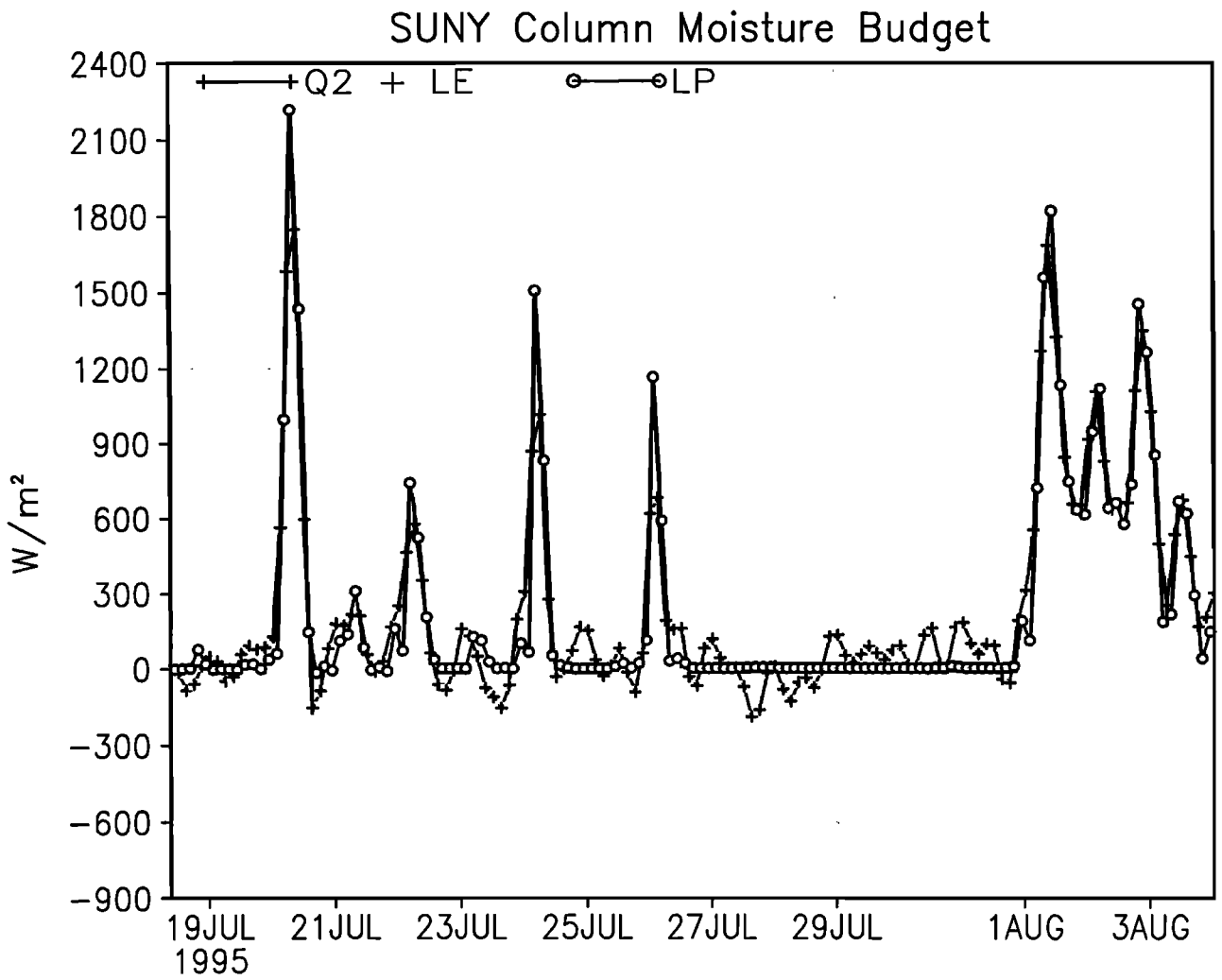


**Figure 3.** Column moisture budget (in W $m^{-2}$ of latent heat) according to the (a) SUNY and (b) LLNL objective analyses. $Q2$ is the latent heat of evaporation multiplied by the column integral of the apparent moisture sink. $LP$ and $LE$ are the latent heat of evaporation multiplied by the precipitation rate and evaporation rate, respectively.

rather than predict the cloud water mixing ratio and hence are less sensitive to the cooling rate. Column cloud ice is also reduced for most models, being enhanced somewhat in the PNNL simulation but reduced in the ECHAM simulation.

The changes in the cloud fields also influence the radiative flux fields. Plate 15 compares the simulated and observed upward solar flux at the top of the atmosphere. The agreement with observations is substantially improved over the baseline experiment (see Plate 9) at times for the CSU and McRAS models. Although none of the models simulate as much upward solar flux as is observed during the disturbed period August 1–3, all models simulate a larger flux during the disturbed period than at any other time. Nudging also improves the simulation of the outgoing longwave radiation (Plate 16). The errors are reduced for almost all models almost all of the time compared to the baseline experiment (see Plate 10). Only the Rutgers simulated OLR is not improved in any respect. The low OLR bias during the disturbed period and at other times is greatly reduced for most models. The McRAS simulation with nudging misses much of the observed low OLR episodes that the simulation without nudging captured successfully.

Perhaps the field most sensitive to nudging is the precipitation rate. For some models, precipitation is substantially reduced by nudging. For example, the precipitation rate for the ECHAM model is reduced from 5.96 kg $m^{-2}$ $d^{-1}$without nudging to 0.41 kg $m^{-2}$ $d^{-1}$with nudging. This response is due to the large moist bias in the simulation without nudging. Nudging dries the atmosphere, replacing precipitation as the primary moisture sink for the atmosphere.

This interpretation is complicated by the influence of temperature on condensation. For example, precipitation simulated by the NCAR SCM increases with nudging, not because of a dry bias in the baseline simulation

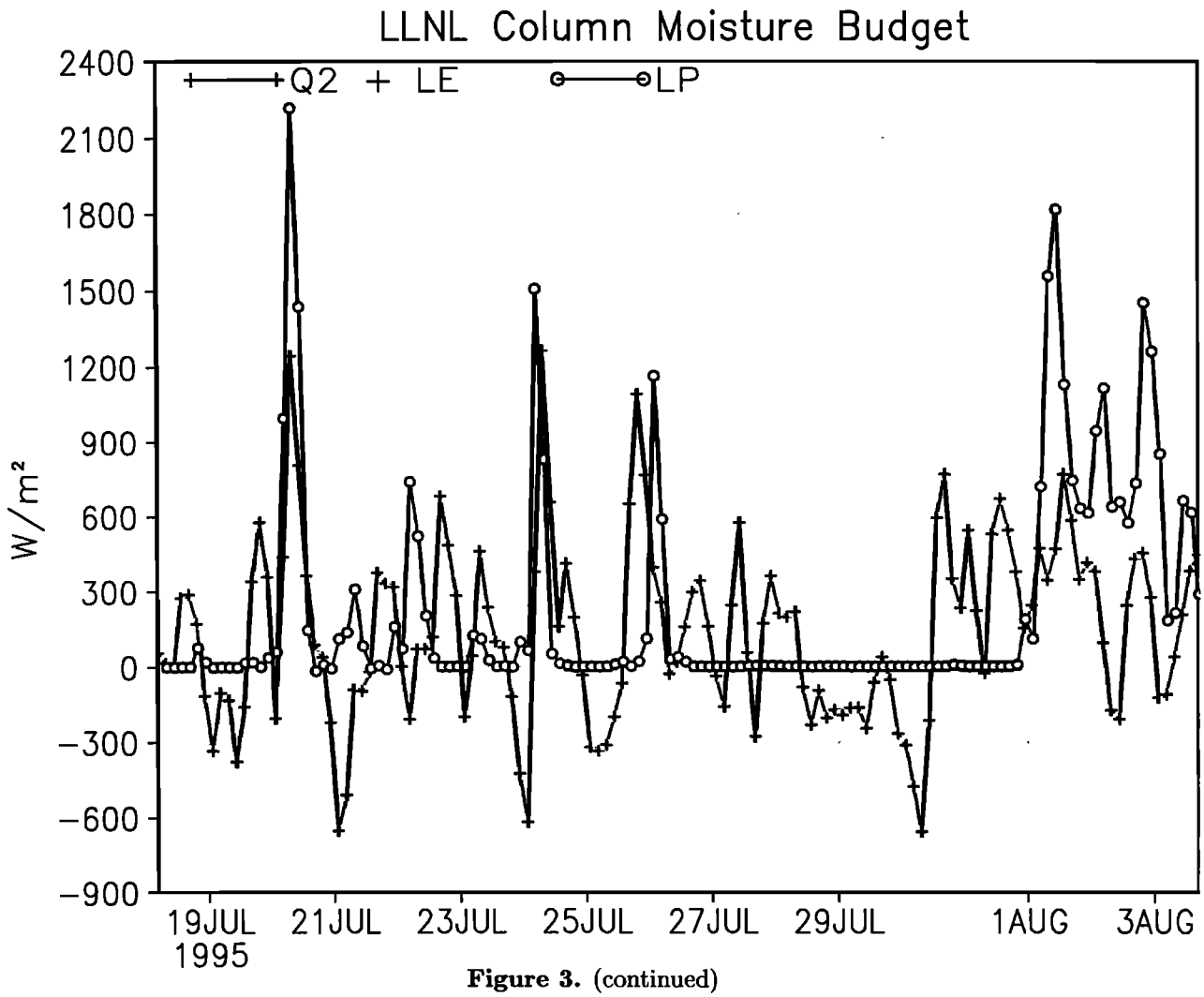


**Figure 3.** (continued)

(it is actually somewhat too moist) but because of a large warm bias. Nudging cools the simulation, which produces more condensation and hence large-scale precipitation. Similarly, precipitation simulated by the Rutgers SCM decreases with nudging because the simulation without nudging is too cool. Thus biases in both temperature and moisture must be considered when anticipating the impact of nudging on precipitation.

One criticism of nudging is that it introduces unphysical terms into the budgets of the nudged variables. The nudging term should be much smaller than other terms in the heat and moisture budgets if the temperature and specific humidity are predicted accurately without nudging. This is the case, for example, in the PNNL simulations, in which the temperature and moisture nudging terms are typically 1 order of magnitude less than other terms in the column heat and moisture balances. However, if temperature or humidity are simulated poorly without nudging, then the nudging term will be quite important in simulations by the same model with nudging. This is illustrated in Plates 17 and 18, which show the column heat and moisture budgets for the CCCma simulation with nudging. Recall that according to Plates 3 and 4 the errors in the temperature and humidity simulated by the CCCma SCM without nudging were quite large; the nudging terms in the CCCma nudging simulation are therefore large. Nudging of temperature is typically 200–400 W $m^{-2}$ and occasionally exceeds 1000 W $m^{-2}$, usually larger than the radiative heating and often comparable to the dynamic heating and the apparent heat source. Nudging of moisture is typically 100–200 W $m^{-2}$ and sometimes exceeds 1000 W $m^{-2}$, often as large as the dynamic moistening and occasionally as large as the apparent moisture sink. This suggests that while nudging might be useful for models when simulations without nudging do not stray far from observations, it should not be used to correct serious biases in models. As shown by *Ghan et al.* [1999], nudging can hide errors in the treatment of processes that influence the fields being nudged and hence should only be used to correct for errors in the SCM forcing or to suppress sensitive dependence on initial conditions [*Hack and Pedretti,* 1999]. As noted by *Randall and Cripe* [1999], nudging does not hide the problems in the model but simply changes the manifestation of the problems. The precipitation rate ap-

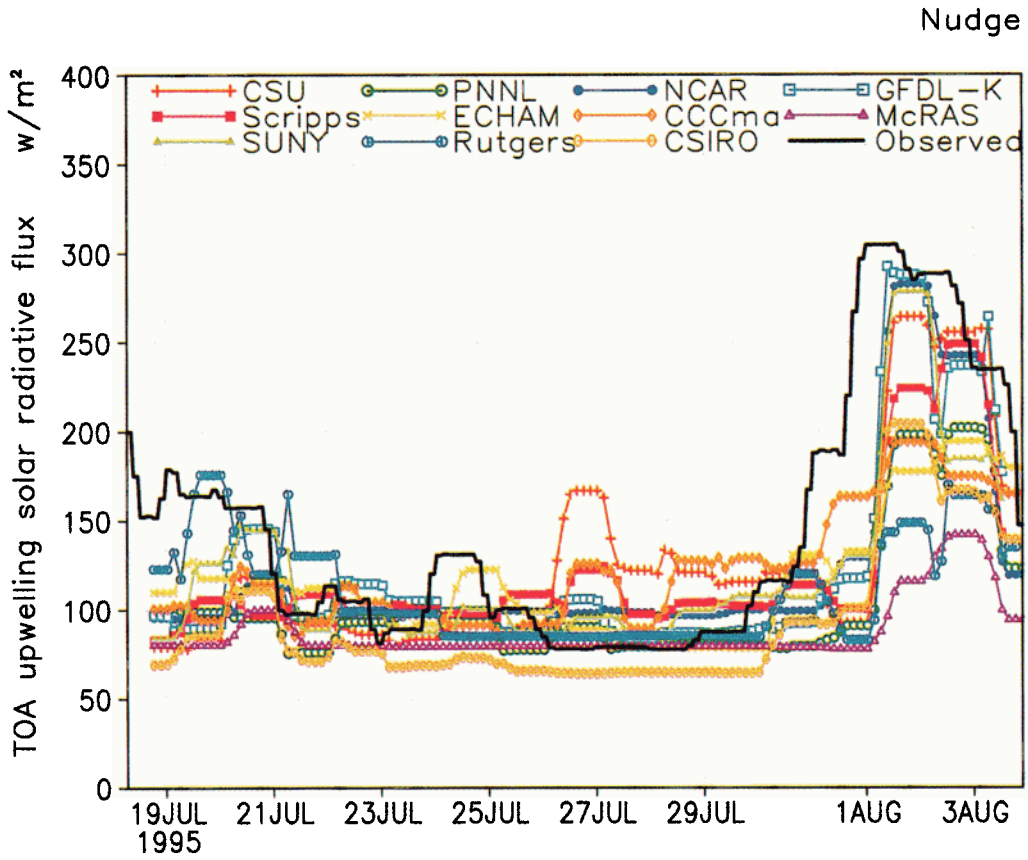


**Plate 15.** Upward 24 hour running mean solar radiative flux at the top of the atmosphere (W $m^{-2}$) as observed and as simulated by each model driven by the forcing shown in Plates 1 and 2 with nudging toward the analyzed temperature and humidity.

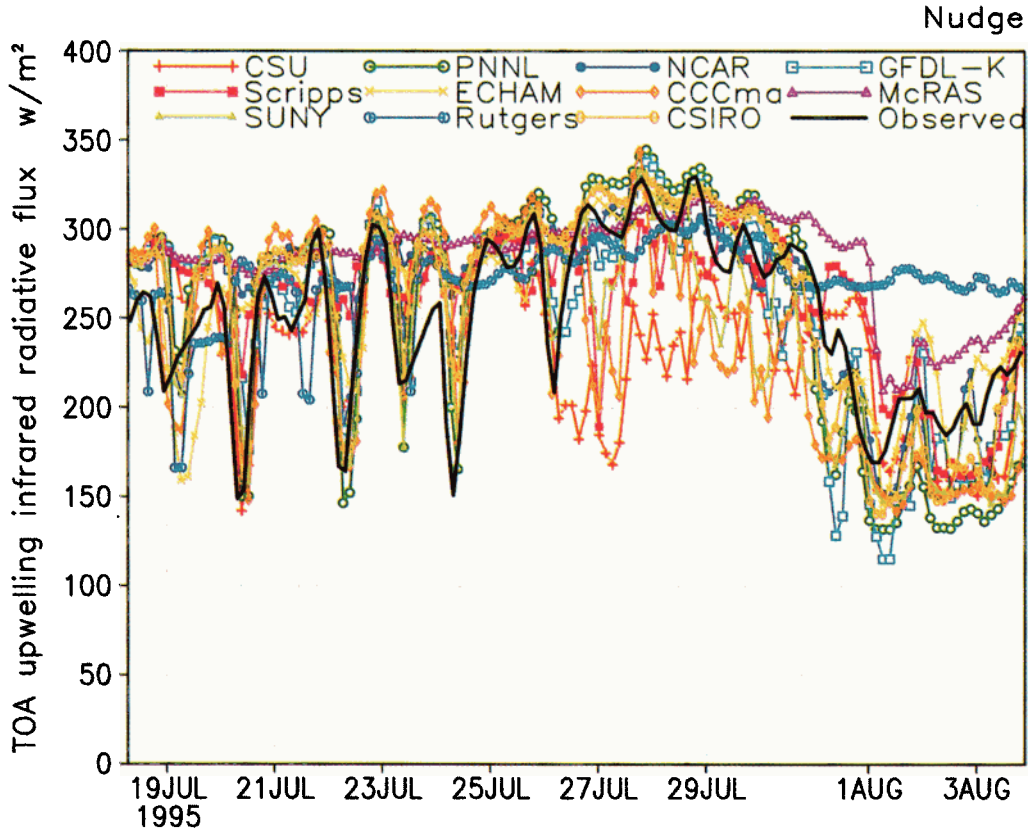


**Plate 16.** Outgoing longwave radiative flux at the top of the atmosphere (W $m^{-2}$) as observed and as simulated by each model driven by the forcing shown in Plates 1 and 2 with nudging toward the analyzed temperature and humidity.

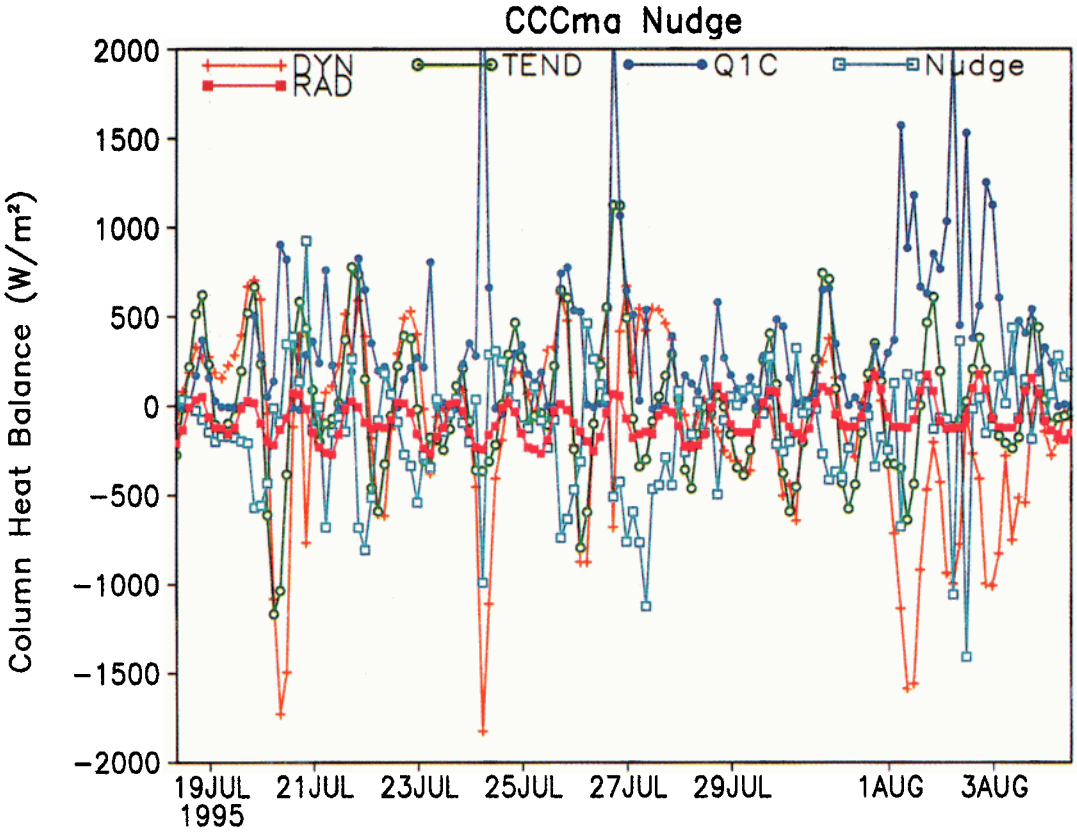


**Plate 17.** Column heat balance (W $m^{-2}$) simulated by the CCCma model driven by the forcing shown in Plates 1 and 2 with nudging toward the analyzed temperature and humidity.

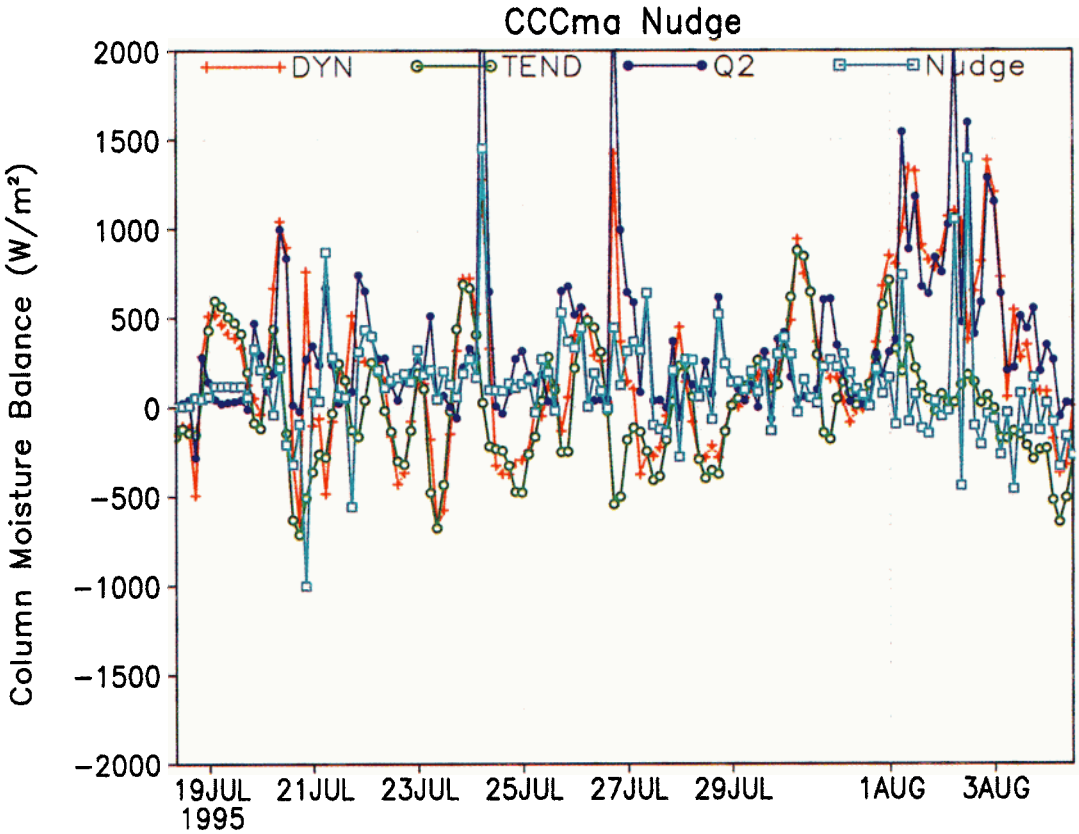


**Plate 18.** Column moisture balance (in W $m^{-2}$ of latent heat) simulated by the CCCma model driven by the forcing shown in Plates 1 and 2 with nudging toward the analyzed temperature and humidity.

pears to be the field most sensitive to the application of nudging and hence should be regarded as a key diagnostic of problems with the model. By applying nudging, the large drifts away from plausible temperature and humidity profiles are avoided, so the parameterizations can be tested under more realistic conditions.

### 5.4. Vertical Aadvective Tendency

As discussed in section 2.1, the vertical advective tendency can be either prescribed from the objective analysis (the baseline treatment) or calculated by the model from the analyzed vertical velocity and the simulated profile of the advected field (experiment VADV). Here we consider the sensitivity of the SCM and CEM simulations to the treatment of the vertical advection term by comparing the baseline simulations with experiment VADV (see Table 1). The differences in the 18 day means of key fields (Tables 10–17) are generally smaller than the differences between the baseline simulations and the simulations drive by the LLNL objective analysis, but are not negligible and exceed the baseline–LLNL differences for some fields and models. For example, the precipitation rate (Table 14) is reduced by a factor of 2–3 for the McRAS and Rutgers SCMs in experiment VADV, and the column water vapor (Table 11) is increased by 20% for the PNNL and Scripps SCMs. The CEM is less sensitive to the treatment of the large-scale vertical advection than most SCMs for most fields.

The issue of improvement of the results with interactive versus prescribed vertical advection is very complicated. Some models show some improvement at selected levels (e.g., CSU, PNNL), or no improvement at all (e.g., McRAS, Scripps and SUNY). There is a general improvement for the CEM for runs with EBBR fluxes but not for runs with the SiB2 fluxes. These results suggest there is no systematic improvement in the simulations when vertical advection is calculated from the analyzed vertical velocity and simulated profiles rather than prescribed from the analyses. Thus the prescription of the total advective forcing in SCM and CEM comparison studies [*Redelsperger et al.*, 1998; *Bechtold et al.*, 1999] is preferred because the total advective tendency is identical among the models.

## 6. Conclusions

As the first in a series of planned comparisons using ARM data, this investigation has revealed much about the feasibility of such a study, about the sensitivity to analysis method and to the forcing method, about the value of involving multiple and diverse models, about the model performance and about the models themselves. Here we summarize our main conclusions and reflect on the direction of our future work.

1. Advective forcing over midlatitude continents (specifically at the ARM southern Great Plains site) can be prescribed accurately enough to distinguish errors due to model deficiencies from errors due to advective forcing errors. The spatial and temporal density of profiling measurements is as high at the SGP site during IOPs as anywhere. The combination of the profile measurements and surface and top-of-atmosphere measurements of the energy and water balance are critical to the analysis of the forcing required to drive the model simulations.

2. The SUNY variational analysis method for determining the lateral boundary conditions yields superior simulations compared with the conventional LLNL analysis. This should not be surprising because the variational method uses additional information about the surface and top-of-atmosphere energy and moisture balance to provide additional constraints on the analyzed lateral boundary conditions. The improvement is particularly evident in the simulated humidity, precipitation, and to a lesser extent in the simulated radiative fluxes.

3. There is no systematic dependence of the simulations on whether the vertical advective tendencies of temperature and humidity are prescribed from the analysis or calculated from the analyzed vertical velocity and simulated vertical profiles of temperature and humidity. The former treatment is therefore preferred for future studies because it ensures that all simulations are driven by the same total advective tendencies.

4. The sensitivity of the simulations to the prescribed surface fluxes is rather weak for all models. However, this conclusion might be different for another study period.

5. The simulations by the cloud ensemble model are generally superior to those by the single-column models. The errors in simulated temperature and humidity are generally lower at all times and at all levels. The errors in simulated precipitation and longwave radiative flux at the top of atmosphere are also lower at all times, but the CEM errors in shortwave flux at the top of atmosphere are as large as in the SCM simulations. Although the CEM simulations are dependent on the parameterizations of turbulence, cloud microphysics, and cloud optical properties, the ability of the CEM to explicitly resolve convective circulations and its apparent superiority in the simulation of most fields establishes it as a reference model for evaluating SCM simulations of fields not observed or under conditions when the forcing errors are too large to permit evaluation of simulated fields by comparison with measurements. However, the bias in the CEM shortwave fluxes needs to be corrected, and tests for other locations and periods are needed to determine whether the CEM just happened to perform well for this particular location and period.

6. Intercomparison of simulations helps to identify errors due to errors in the boundary conditions used to drive the simulations. Consistent errors across all models (CEM as well as SCM) indicate errors in the forcing, while errors particular to individual models indicate errors in the models.

7. Application of nudging of temperature and humid-

ity to SCM simulations is helpful in reducing sensitive dependence on initial conditions and in correcting for errors in the forcing but can be also hide errors in the parameterizations being evaluated. The reductions in errors in temperature and humidity leads to improvements in the simulated clouds and radiative fluxes but also produces larger errors in the simulated precipitation rate. The response to nudging can often be anticipated from the temperature and humidity biases simulated without nudging. If the contribution of the nudging terms to the heat and moisture budgets is comparable to the advective tendencies, then nudging should not be used.

8. Given the different treatments of a variety of processes in the models, it is often difficult to explain many simulation differences in terms of differences in model physics. However, in some cases model problems were identified and corrected through the process of intercomparison and evaluation, and in other cases model problems have been identified and remain to be corrected. In conventional validation of the models run in three-dimensional climate mode the problems might have passed unnoticed. Further resolution of the differences between simulations will require a systematic substitution of the parameterizations of all processes, which although beyond the scope of this paper is clearly the next step toward understanding the cause(s) of the different biases in the simulations.

The next case to be considered will be case 3: June 18 to July 18 1997. This case features a much wider suite of measurements for evaluation, including cloud measurements from aircraft and from a combination of cloud radar, microwave radiometer, ceilometer, and lidar. A wider cast of models is being recruited, including more SCMs and CEMs from the GCSS community and operational forecast models from the numerical weather prediction community. Ensembles of simulations will be required for the SCMs, given their tendency toward sensitive dependence on initial conditions. Parameterizations of all processes will be systematically substituted to completely reconcile differences between simulations by different models.

Subsequent cases will move on to other seasons (when horizontal advection plays a greater role) and to the other ARM sites in the tropical west Pacific and north slope of Alaska, where IOPs are planned for 1999.

**Acknowledgments.** This work was supported at PNNL by the U.S. Department of Energy Atmospheric Radiation Measurement program, which is part of the DOE Biological and Environmental Research program. Pacific Northwest National Laboratory is operated for the DOE by Battelle Memorial Institute under contract DE-AC06-76RLO 1830. Work at CSU was supported by the ARM program under grant DE-FG03-95ER61968. Work at GSFC was supported by Ken Bergman at NASA Headquarters. Work at Rutgers was funded by DOE National Institute for Global Environmental Change (NIGEC) through the NIGEC Great Plains Regional Center at the University of Nebraska-Lincoln (DOE cooperative agreement No. DE-FC03-90ER61010). Work at LLNL was supported by the ARM program, and was performed under the auspices of the U.S. Department of Energy by the Lawrence Livermore National Laboratory under contract W-7405-Eng-48. Work at the University of Utak was supported by the ARM program under grant DE-FG03-94ER61769. Work at NCAR was supported by the DOE Climate Change Prediction program and by the DOE ARM program. NCAR is sponsored by the National Science Foundation. Work at SUNY was supported by the DOE ARM program under grant DEFG0298ER62570, and by NSF under grant ATM9701950 to SUNY at Stony Brook. Work at Scripps was supported in part by the Department of Energy under grant DOEDE-FG03-97-ER62338, the National Oceanic and Atmospheric Administration under grant NA77RJO453, and the National Science Foundation under grant ATM-9613764. Work at Dalhousie University was funded by NSERC. The work at CSIRO was partly funded through Australia's National Greenhouse Research program. Doug Sisterton of Argonne National Laboratory provided the map of the ARM SGP site; ANL is managed and operated by the Univ. of Chigago for the U.S. Dept. of Energy under contract W-31-109-ENG-38. The CEM simulations were performed at the National Energy Research Supercomputer Center, Berkeley, CA. Financial support does not constitute an endorsement by DOE of the views expressed in this article.

## References

Abdella, K. and N. McFarlane, A new second order turbulence closure scheme for the planetary boundary layer, *J. Atmos. Sci., 54,* 1850–1867, 1997.

Barnes, S.L., A technique for maximizing details in numerical weather map analysis, *J. Appl. Meteorol., 3,* 396–409, 1964.

Bechtold, P., *et al.*, A GCSS model intercomparison for a tropical squall line observed during TOGA-COARE, part II, Intercomparison of SCMs and with CRM, *Q. J. R. Meteorol. Soc.*, in press, 1999.

Betts, A.K , and M.J. Miller, A new convective adjustment scheme. part II, Single column model tests using GATE wave, BOMEX, ATEX and arctic air-mass data sets. *Q. J. R. Meteorol. Soc., 112,* 693–709, 1986.

Brinkop S., and E. Roeckner, Sensitivity of a general circulation model to parameterizations of cloud-turbulence interactions in the atmospheric boundary layer, *Tellus, Ser. A, 47,* 197–220, 1995.

Browning, K. A., The GEWEX Cloud System Study (GCSS), *Bull Am. Meteorol. Soc., 74,* 387–399, 1993.

Caracena, F., Analytic approximation of discrete field samples with weighted sums and the gridless computation of field derivatives, *J. Atmos. Sci., 44,* 3753–3768, 1987.

Chou, M.-D., and M. J. Suarez, An efficient thermal infrared radiation parameterization for use in general circulation models, *NASA Tech. Memo. 104606, 3,* 85 pp., 1994.

Chou, M.-D., M. J. Suarez, C.-H. Ho, M.-H. Yan, and K.-T. Lee, Parameterization for cloud overlapping and shortwave single scattering properties for use in general circulation and cloud ensemble models, *J. Clim., 11,* 202–214, 1998.

Chou, M.-D., K. -T., Lee, and S. -C., Tsay, Parameterization of cloud longwave scattering for use in atmospheric models, *J. Clim., 12,* 159–169, 1999

Ding P., and D. A. Randall, A cumulus parameterization with multiple cloud base levels, *J. Geophys. Res., 103,* 11,341–11,353, 1998.

Doran, J.C., J.M. Hubbe, J.C. Liljegren, W.J. Shaw, G.J. Collatz, D.R. Cook, and R.L. Hart, A technique for determining the spatial and temporal distributions of sur-

face fluxes of heat and moisture over the Southern Great Plains Cloud and Radiation Testbed, *J. Geophys. Res., 103,* 6109–6121, 1998.

Ebert, E.E., and J.A. Curry, A parameterization of ice cloud optical properties for climate models, *J. Geophys. Res., 97,* 3831–3836, 1992.

Fouquart, Y. and B Bonnel, Computations of solar heating of the Earth's atmosphere: A new parameterization, *Beitr. Phys. Atmos., 53,* 35–62, 1980.

Fowler, L.D., and D.A. Randall, Liquid and ice cloud microphysics in the CSU general circulation model, II, Impact on cloudiness, the Earth's radiation budget, and the general circulation of the atmosphere, *J. Clim., 9,* 530–560, 1996.

Fowler, L.D., D.A. Randall, and S.A. Rutledge, Liquid and ice cloud microphysics in the CSU general circulation model, I, Model description and simulated microphysical processes, *J. Clim., 9,* 489–529, 1996.

Ghan, S. J., L. R. Leung, and Q. Hu, Application of cloud microphysics to NCAR CCM2, *J. Geophys. Res., 102,* 16,507–16,527, 1997.

Ghan, S.J., L.R. Leung, and J. McCaa, A comparison of three different modeling strategies for evaluating cloud and radiation parameterizations, *Mon. Weather. Rev., 127,* 1967–1984, 1999.

GCSS Science Team, The GEWEX Cloud System Study, *Bull. Am. Meteorol. Soc., 74,* 387–400, 1993.

Gregory, D., and P. R. Rowntree, A mass flux convection scheme with representation of cloud ensemble characteristics and stability-dependent closure, *Mon. Weather. Rev., 118,* 1483–1506, 1990.

Hack, J J., Parameterization of moist convection in the National Center for Atmospheric Research community climate model (CCM2), *J. Geophys. Res., 99,* 5551–5568, 1994.

Hack, J. J., Sensitivity of the simulated climate to a diagnostic formulation for cloud liquid water, *J.Clim., 11,* 1497–1515, 1998.

Hack, J.J., and J.A. Pedretti, Assessment of solution uncertainties in single-column modeling frameworks, *J. Clim.,* in press, 1999.

Hack, J. J., B. A. Boville, B.P. Briegleb, J.T. Kiehl, P.J. Rasch, and D.L Williamson, Description of the NCAR Community Climate Model (CCM2). *NCAR Tech. Note, NCAR TN-336-STR,* 108 pp., National Center for Atmospheric Research, Boulder, Colo., 1993.

Hack, J.J., J.A. Pedretti, and J.C. Petch, SCCM User's Guide. (http://www.cgd.ucar.edu/cms/sccm/sccm.html), 1998.

Harshvardhan, *et al.*, A fast radiation parameterization for general circulation models, . *Geophys. Res., 92,* 1009–1016, 1987

Holtslag, A. A. M., and B. A. Boville, Local versus nonlocal boundary-layer diffusion in a global climate model, *J. Clim., 6,* 1825–1842, 1993.

Helfand, H. M., and J. C. Lebraga, Design of a non-singular level 2.5 second order closure model for prediction of atmospheric turbulence, *J. Atmos. Sci., 45,* 113–132, 1988.

Iacobellis, S.F., and R.C.J. Somerville, Diagnostic modeling of the Indian monsoon onset, part I, Model description and validation, *J. Atmos. Sci., 48,* 1948–1959, 1991.

Kiehl, J. T., B. Boville, B. Briegleb, J. Hack, P.Rasch, and D. Williamson, Description of the NCAR Community Climate Model (CCM3). *NCAR Tech. Note, NCAR TN-420-STR,* 151 pp., National Center for Atmospheric Research, Boulder, Colo., 1996.

Kiehl, J.T., J.J. Hack, G.B. Bonan, B.A. Boville, D.L. Williamson, and P.J Rasch, The National Center for Atmospheric Research Community Climate Model: CCM3, *J. Clim., 11,* 1131–1149, 1998.

Krueger, S. K., Numerical simulation of tropical cumulus clouds and their interaction with the subcloud layer, *J. Atmos. Sci., 45,* 2221–2250, 1988.

Krueger, S.K., Q. Fu, K.N. Liou, and H.-N. Chin, Improvements of an ice-phase microphysics parameterization for use in numerical simulations of tropical convection, *J. Appl. Meteorol. 34,* 281–287, 1995.

Lacis, A.A., and J.E. Hansen, A parameterization for the absorption of solar radiation in the Earth's atmosphere, *J. Atmos. Sci., 31,* 118–133, 1974.

Leach, M.J., J. Yio, and R.T. Cederwall, Estimation of errors in objectively analyzed fields and sensitivity to number and spacing of stations, in *Proceedings of the Sixth Annual Atmospheric Radiation Measurement (ARM) Science Team Meeting, DOE CONF-9603149 UC-402,* pp. 149–151, Department of Energy, Washington, D.C., 1997.

Lesht, B.M., and J.C. Liljegren, Comparison of precipitable water vapor measurements obtained by microwave radiometry and radiosondes at the Southern Great Plains Cloud and Radiation Testbed, in *Proceedings of the Sixth Atmospheric Radiation Measurement (ARM) Science Team Meeting,* March 4-7, 1996, San Antonio, Texas, pp. 165–168, available from NTIS as CONF-9603149, 1997.

Lin, Y. -L., R. D. Farley, and H. D. Orville, Bulk parameterization of the snow field in a cloud model, *J. Clim. Appl. Meteorol., 22,* 1065–1092, 1983.

Lohmann, U., and E. Roeckner, Design and performance of a new cloud microphysics scheme developed for the ECHAM general circulation model, *Clim. Dyn., 12,* 557–572, 1996.

Lohmann, U., N. McFarlane, L. Levkov, K. Abdella, and F. Albers, Comparing different cloud schemes of a single column model by using mesoscale forcing and nudging technique, *J. Clim., 12,* 438–461, 1999.

Lord, S. J., H. E. Willoughby, and J. M. Piotrowicz, Role of a parameterized ice-phase microphysics in an axisymmetric, non-hydrologic tropical cyclone model *J. Atmos. Sci., 41,* 2836–2848, 1984.

Louis, J.-F , A parameteric model of vertical eddy fluxes in the atmosphere, *Boundary Layer Meteorol., 17,* 187–202, 1979.

Mace, G.G., and T.P. Ackerman, Assessment of error in synoptic scale diagnostics derived from wind profiler and radiosonde network data, *Mon. Weather Rev., 124,* 1521–1534, 1996.

Minnis, P., and W. L. Smith, Jr., Cloud and radiative fields derived from GOES-8 during SUCCESS and the ARM-UAV Spring 1996 Flight Series, *Geophys. Res. Lett., 25,* 1113–1116, 1998,.

Minnis, P., W.L. Smith, D.P. Garber, J.K. Ayers, and D.R. Doelling, *Cloud properties derived from GOES-7 for spring 1994 ARM intensive observing period using version 1.0.0 of ARM satellite data analysis program, NASA Ref. Publ. 1366,* 1995.

Moncrieff, M.W., S.K. Krueger, D. Gregory, J.-L. Redelsperger, and W.-K. Tao, GEWEX Cloud System Study (GCSS) Working Group 4: Precipitating convective systems, *Bull. Am. Meteorol. Soc., 78,* 831–845, 1997.

Moorthi, S., and M. J. Suarez, Relaxed Arakawa-Schubert: A parameterization of moist convection for general circulation models. *Mon. Weather Rev., 120,* 978–1002, 1992.

Morcrette, J. J., Description of the radiative scheme in the ECMWF model, *Tech. Rep. 165,* 26 pp., Eur. Cent. for Medium-Range Weather Forecasts, REading, England, 1989.

Nordeng, T. E., Extended versions of the convective param-

eterization scheme at ECMWF and their impact on the mean and transient activity of the model in the tropics, *Tech. Memo. 206*, 41 pp., Eur. Cent. for Medium Range Weather Forecasts, Reading, England, 1994.

O'Brien, J.J., Alternative solutions to the classical vertical velocity problem, *J. Atmos. Sci., 9*, 197–203, 1970.

Pan, D. -M., and D. A. Randall, A cumulus parameterization with a prognostic closure, *Q. J. R. Meteorol. Soc., 125*, 949–982, 1998

Petch, J.C., and J. Dudhia, The importance of horizontal advection of hydrometeors in a single column model, *J. Clim., 11*, 2437–2452, 1998.

Randall, D.A., and D.G. Cripe, Alternative methods for specification of observed forcing in single-column models and cloud system models, *J. Geophys. Res.*, in press, 1999

Randall, D.A., K.-M. Xu, R.J.C. Somerville, and S. Iacobellis, Single-column models and cloud ensemble models as links between observations and climate models, *J. Clim., 9*, 1683–1697, 1996.

Redelsperger, J.L., *et al.*, A GCSS model intercomparison for a tropical squall line observed during TOGA-COARE, part 1, Cloud-resolving models, *Q. J. R. Meteorol. Soc.*, in press, 1998.

Roeckner, E., *et al.*, The atmospheric general circulation model ECHAM4: Model description and simulation of the present-day climate, *Tech. Rep. 218*, Max Planck Inst. for Meteorol., Hamburg, Germany, 1996.

Rotstayn, L.D., A physically based scheme for the treatment of stratiform clouds and precipitation in large-scale models, I, Description and evaluation of the microphysical processes, *Q. J. Ry. Meteorol. Soc., 123*, 1227–1282, 1997.

Rotstayn, L D., B. F Ryan, and J. J. Katzfey, A scheme for calculation of the liquid fraction in mixed-phase stratiform clouds in large-scale models, *Mon. Weather Rev.*, in press, 1999.

Schwarzkopf, M. D. and S. B. Fels, The simplified exchange method revisited: An accurate rapid method for computation of IR cooling rates and fluxes, *J. Geophys. Res., 96*, 9075–9096, 1991.

Sellers, P.J., Y. Mintz, Y.C. Sud, and A. Dalcher, A simple biosphere model (SiB) for use within general circulation models, *J. Atmos. Sci, 43*, 305–331, 1986.

Sellers, P.J., D.A. Randall, G.J. Collatz, J.A. Berry, C.B. Field, D.A. Dazlich, C. Zhang, G.D. Collelo, and L. Bounoua, A revised land surface parameterization (SiB2) for atmospheric GCMs, part I, Model formulation, *J. Clim., 9*, 676–705, 1996.

Slingo, A , A GCM parameterization for the shortwave radiative properties of water clouds, *J. Atmos. Sci., 46*, 1419–1429. 1989.

Slingo, J. M., The development and verification of a cloud prediction scheme for the ECMWF model, *Q. J. R. Meteorol. Soc., 113*, 899–927, 1987.

Smith, R.N.B., A scheme for predicting layer clouds and their water content in a general circulation model, *Q. J. R. Meteorol. Soc., 116*, 435–460, 1990.

Stenchikov, G., and A. Robock, Diurnal asymmetry of climatic response to increased $CO_2$ and aerosols: Forcings and feedbacks, *J. Geophys. Res., 100*, 26,211–26,227, 1995.

Stephens, G.L., Radiation profiles in extended water clouds, II, Parameterization schemes, *J. Atmos. Sci., 35*, 2123–2132, 1978.

Stokes, G.M., and S.E. Schwartz, The Atmospheric Radiation Measurement (ARM) program: Programmatic background and design of the Cloud and Radiation Testbed, *Bull. Am. Meteorol. Soc., 75*, 1201–1221, 1994.

Suarez, M. J., A. Arakawa, and D. A. Randall, Parameterization of the planetary boundary layer in the UCLA general circulation model: Formulation and results, *Mon. Weather Rev., 111*, 2224–2243, 1983.

Sud, Y. C., and G. K. Walker, Microphysics of clouds with the Relaxed Arakawa-Schubert Scheme (McRAS), part I, Design and evaluation with GATE phase III data, *J. Atmos. Sci., 56*, 3196–3220, 1999

Sud, Y.C., and G. K. Walker, Microphysics of clouds with the Relaxed Arakawa-Schubert Scheme (McRAS), part II, Implementation and Performance in GEOS II GCM, *J. Atmos. Sci., 56*, 3221–3240, 1999.

Takacs, L. L., A. Molod, and T. Weng, Goddard Earth Observing System (GEOS) General Circulation Model (GCM) Version 1, *NASA Tech. Memo. 104606*, Vol. 1, 97 pp., 1994.

Tiedtke, M., A comprehensive mass flux scheme for cumulus parameterization in large-scale models, *Mon. Weather Rev., 117*, 1779–1800, 1989.

Tiedtke, M., Representation of clouds in large-scale models, *Mon. Weather Rev., 121*, 3040–3061, 1993.

Xu, K.-M., and S. K. Krueger, Evaluation of cloudiness parameterizations using a cumulus ensemble model, *Mon. Weather Rev., 199*, 342–367, 1991.

Xie, S. C., Single-Column Modeling: methodology and application to the evaluation of cumulus convection schemes in GCMs, Ph.D thesis, 126 pp., State Univ. of N. Y. at Stony Brook, December 1998.

Xu, K.-M., and D. A. Randall, Impact of interactive radiative transfer on the macroscopic behavior of cumulus ensembles, part I, Radiation parameterization and sensitivity test, *J. Atmos. Sci., 52*, 785–799, 1995.

Xu, K.-M., and D. A. Randall, Explicit simulation of cumulus ensembles with the GATE Phase III data: Comparison with observations, *J. Atmos. Sci., 53*, 3710–3736, 1996.

Xu, K.-M., and D. A. Randall, Explicit simulation of midlatitude cumulus ensembles, part I, Comparison with ARM data, *J. Atmos. Sci.* in press, 1998,

Yanai, M., S. Esbensen, and J. Chu, Determination of bulk properties of tropical clusters from large-scale heat and moisture budgets, *J. Atmos. Sci., 30*, 611-627, 1973.

Zhang, G. J., and N. A. McFarlane, Sensitivity of climate simulations to the parameterization of cumulus convection in the Canadian Climate Center general circulation model *Atmos.-Ocean, 33*, 407–446, 1995.

Zhang, M.H., and J.L. Lin, Constrained variational analysis of sounding data based on column-integrated budgets of mass, heat, moisture and momentum: Approach and application to ARM measurements, *J. Atmos. Sci., 54*, 1503–1524, 1997

Zhang, M.H., J.L. Lin, R.T. Cederwall, J.J. Yio, and S.C. Xie, Objective analysis of the ARM IOP data: Method and sensitivity, *Mon. Weather Rev.*, in press, 1999.

S. Ghan, Pacific Northwest National Laboratory, Richland, WA 99352. (steve.ghan@pnl.gov)

D. Randall, K.-M. Xu, and D. Cripe, Department of Atmospheric Science, Colorado State University, Fort Collins, CO 80523

R. Cederwall, S. Xie, and J. Yio, Lawrence Livermore National Laboratory, Livermore, CA 94550.

J. Hack and J. Pedretti, National Center for Atmospheric Research, P.O. Box 3000, Boulder, CO 80307.

S. Iacobellis and R. Somerville, Scripps Institution of

Oceanography, University of California, Dept. 0224, La Jolla, CA 92093

S. Klein, Geophysical Fluid Dynamics Laboratory, Princeton, NJ 08542.

S. Krueger, Department of Meteorology, University of Utah, Salt Lake City, UT 84112.

U. Lohmann, Department of Physics and Oceanography, Dalhousie University, Halifax, Nova Scotia.

G. Stenchikov and A. Robock, Department of Environmental Sciences, Rutgers University, New Brunswick, NJ, 20742.

L. Rotstayn, CSIRO Atmospheric Research, PMB 1, Aspendale, Vic. 3195 Australia.

Y. Sud and G. Walker, Goddard Space Flight Center, Greenbelt, MD, 20771.

M. Zhang, Institute of Terrestrial and Planetary Atmospheres, State University of New York, Stony Brook, NY 11794.

(Received March 29, 1999; revised August 12, 1999; accepted September 9, 1999.)